1.4-EV LUMINESCENCE IN P-TYPE CADMIUM TELLURIDE SINGLE CRYSTALS

By

HECTOR LUIS COTAL

Bachelor of Science

in Arts and Sciences

Oklahoma State University

Stillwater, Oklahoma

1986

Submitted to the Faculty of the Graduate
College of the Oklahoma State Univesity
in partial fulfillment of
the requirements for
the Degree of
MASTER OF SCIENCE
July, 1990

Illinois
1990
C8430
cop 2

Oklahoma State Univ. Library

1.4-EV LUMINESCENCE IN P-TYPE CADMIUM TELLURIDE SINGLE CRYSTALS

Thesis Approved:

Thesis Adviser

Larry E. Halliburton

James P. Wikswo

Norman N. Durham

Dean of the Graduate College

1370470

ACKNOWLEDGMENTS

I would like to express sincere gratitude to Dr. S. W. S. McKeever for his patience, advice and support throughout my research studies. Also, I am greatly indebted to him for giving me an opportunity to work in his lab and for the many fruitful discussions we had. I would also like to thank Dr. L. E. Halliburton, Dr. J. P. Wicksted and Dr. J. J. Martin for being members of my thesis committee. Discussions with them were enlightening and helpful.

Many thanks are in order for Brian Markey for numerically solving the coupled, differential equations. His help with some of the software is greatly appreciated. Also, I would like to thank Dr. J. D. Vitek for allowing me to enter the graduate program, and all the people at Oklahoma State University who helped me throughout my graduate studies.

Foremost of all, I wish to give special thanks to my wife, Sharon, for her encouragement and support throughout my entire graduate program. A special debt is owed to her for enduring my long hours of study with understanding and patience.

Finally, I would like to thank the Defense Advance Research Project Agency for making this work possible.

TABLE OF CONTENTS

Chapter		Page
I.	INTRODUCTION	1
	Previous Studies	1
	Crystal Structure	6
	Scope of this Study	8
II.	EXPERIMENTAL PROCEDURE	10
	Samples	10
	Spectra Correction	11
	Photoluminescence and Thermal Quenching Spectra	11
	Excitation Intensity Spectra	15
	Time-Resolved Spectra	17
III.	PHOTOLUMINESCENCE AND THERMAL QUENCHING SPECTRA	22
	Introduction	22
	Experimental Results	22
	Discussion	32
IV.	EXCITATION INTENSITY AND TIME-RESOLVED SPECTRA	43
	Introduction	43
	Experimental Results and Discussion	43
	Further Discussion	51
V.	SUMMARY AND CONCLUSIONS	61
LITERATURE CITED		65

LIST OF FIGURES

Figure		Page
1.	A Unit Cube of the Zincblende Structure in Cadmium Telluride.	7
2.	Standard Irradiance Curve of the Quart-Iodine Source	12
3.	Experimental Apparatus for Photoluminescence and Thermal Quenching Spectra.	13
4.	Experimental Apparatus for Excitation Intensity Spectra.	16
5.	Copper Block Arrangement for Holding the Samples in Place	18
6.	Experimental Apparatus for Time-Resolved Spectra.	19
7.	PL Spectrum at 77 K from a Mn-Doped (79 ppm) CdTe Sample.	23
8.	Effects of Etching on the PL Signal from an Undoped CdTe Sample (A) Unetched (B) Etched	26
9.	Thermal Quenching Spectra of the 1.4-eV Emission from the Sample in Fig. 8	29
10.	Arrhenius Plot of the PL Thermal Quenching Data from a Mn-Doped (79 ppm) CdTe Sample. . . .	30
11.	PL Spectrum at 12 K of the 1.4-eV Emission from an Undoped CdTe Sample.	33
12.	PL Spectrum at 77 K from a Sample Grown by the Modified Vapor Phase Transport	37

Figure Page

13. Energy Level Model to Explain the PL Data 39

14. Excitation Intensity Spectra at 77 K from a Mn-Doped (400 ppm) CdTe Sample. 45

15. Dependence of the Emission Intensity on the Excitation Intensity data from the Sample in Fig. 14 (•) and an Undoped Sample (*). 47

16. Time-Resolved Spectra at 77 K of the 1.4-eV Emission from an Undoped CdTe Sample. 49

17. Time-Resolved Spectra at 14 K from the Sample in Fig. 16 50

18. (a) Buildup of I_1 and I_2, and the (b) Decay of I_1 and I_2 During and after Illumination. 55

19. Variation of Steady-State Values of I_1 and I_2 with f. 57

CHAPTER I

INTRODUCTION

Previous Studies

In 1947, single crystals of cadmium telluride (CdTe) were studied for the first time when Frerichs (1) grew these materials for photoconductivity measurements. In 1959 de Nobel (2) studied the radiative recombination mechanisms responsible for the broad-emission band in single-crystal CdTe by means of photoluminescence (PL) and electroluminescence (EL) measurements. Two years later, Thomas (3) used reflectivity measurements to reveal the recombination characteristics of the exciton emission bands in CdTe. Many types of investigations have been made on this material since the pioneering work of these investigators. The reasons for continuing these investigations are due to some of the specific technological applications that have recently become available. For example, since this material has a wide band gap, much effort has been directed toward using it in infrared detectors as a substrate because of its close lattice match with HgCdTe. Other applications include using CdTe in the areas of optoelectonics and integrated optics, and gamma-ray detectors and solar cells (9). Recently, there has been an upsurge of interest by examining PL spectra at 77 K and

low temperature as a means of determining crystal quality, with the aim of improving crystal growth techniques (5,9). Our motivation for studying undoped and manganese-doped CdTe is due to the potential use of this material as a near infrared spatial light modulator. The developement of this type of device would be important for applications in photonics systems including energy generation, communications and information processing.

Before such a device can be developed, however, it is necessary to determine the energies of the localized defect states in order to improve device performance. The presence of these states can affect the nonlinear optical properties of the material in two ways. First, intrinsic states (i.e., real states) within the bandgap can enhance the process of two-photon absorption, and second, trapping of free carriers can give rise to long-lived photorefractive effects and free carrier removal from the delocalized bands. A popular experimental tool to accomplished this is PL spectroscopy which is one of the most powerful experimental techniques for characterizing defect states in materials capable of absorbing light. Much information on the radiative recombination mechanisms can be obtained at 77 K and lower temperatures by using a variety of PL techniques.

In CdTe, two luminescence bands are typically seen at 77 K -- a narrow band at about 1.58 eV and a broad band at about 1.42 eV. The former band is due to free and bound exciton decay. Although the latter band has been frequently observed

to be near 1.42 eV, the peak maximum, nevertheless, has been seen in the range from 1.40 to 1.49 eV (12). This region is commonly termed the 1.4-eV defect emission band and has been seen in samples prepared in a diversity of ways and with a wide range of properties, and occurs in all but the purest samples. At temperatures between 1.8 and 20 K, however, three regions of PL emission are seen. These are the 1.4 to 1.5 eV, the 1.51 to 1.56 eV and the 1.57 to 1.603 eV emission regions. The 1.51 to 1.56 eV and 1.57 to 1.603 eV regions are termed the edge and exciton emission regions, respectively. However, this thesis deals only with the origin of the 1.4-eV defect band.

It is generally observed that, when temperatures are low enough, the defect band usually shows equally spaced emission components due to phonon emission. The separation between the zero-phonon component and its replicas is 21.3 meV corresponding to the energy of longitudinal optical (LO) phonons. Longitudinal acoustical (LA) phonons have also been observed but these usually arise as a result of deep-center electronic transitions (7).

The major interest of this thesis is the origin of the defects giving rise to the 1.4-eV broad-emission band. Understanding how the emission band behaves under different experimental conditions is important for gaining much knowledge on the defect structure. Much work has been directed toward this effort in many CdTe crystals grown by different methods (4-6), or with deviations from stoichiometry and differing

impurity content (7-17). The origin of the emission has been attributed to native defects which are defects intrinsic of the material and may be associated with the accidental contamination of residual impurities during the crystal growth process. Native defects associated with impurities in one way or the other seem to be the origin most commonly accepted for the 1.4-eV emission. The defects involved in the production of the 1.4-eV emission band have been reported as Cd vacancies, Te vacancies, Cd interstitials, Te interstitials, impurity substitution on Cd sites, Cd vacancy-donor complex and surface defects (2,4,7-13). The 1.4-eV emission has been observed in n- and p-type and semi-insulating samples and it has been reported that the emission does not seem to be related to Cd or Te overpressure during the growth process (16).

The source of the electronic transitions responsible for this emission band are still a matter of much debate. Three mechanisms have been suggested in the literature. The first involves transitions of free electrons from the conduction band with trapped hole states or free-to-bound (FB) transitions. The second involves interimpurity transitions or donor-acceptor pair (DAP) recombination, and the third involves electron-hole recombination within a localized center.

It is difficult to decide on any one of the mechanisms just presented based on the data found in the published literature. For instance, the first mechanism fails to explain the shift in energy of the 1.4-eV luminescence band

from excitation intensity and time-resolved experiments when only one hole state or shallow acceptor state is included in a model. From the former experiment, this shift has been generally observed to occur from lower to higher energy as the intensity of the excitation source is increased (4,14,15). From the latter, it has been reported that the shift takes place from higher to lower energy with time after decay of the pulsed excitation source (4). In spite of this, the model appears to work when explaining PL thermal quenching measurements. The problem with the second mechanism is the difficulty in accounting for the measured values of the thermal quenching energies which are of the order of 0.10-0.16 eV (12). This implies that the donor level must be just a few hundreths of an eV below the conduction band. For the DAP model to be valid, it would thus have to consider the donor states as being "thermally disconnected" from the conduction band. This is an unlikely possibility considering the activation energy values obtained from thermal quenching studies. However, the DAP model seems to explain the spectral energy shifts observed from the experiments mentioned above. The third mechanism loosely describes electron-hole recombination within a localized center through an excited state by using the configurational coordinate model (11). However, this analysis seems to explain the interaction of LA phonons with the 1.4-eV defect band but is somewhat irrelevant to the origin of the band which is what these investigators initially set out to do. Difficulties are also apparent when at-

tempts are made to fit the thermal dependencies of the intensity and the Full Width at Half Maximum (FWHM) for the emission band to this model (16,17). The analysis yields fitting constants which are unreasonable and provide no physical insight into the process involved. In addition, the analysis neglects the presence of overlapping peak components considering the asymmetric shape of the emission band observed by these authors.

Finally, it is to be noted that Myers et al. (13) observed that the intensity of the 1.4-eV band is affected dramatically when the samples are polished by different techniques. Consequently, they noted that surface damage was introduced to the sample in various proportions and depended on the polishing technique used. They noted also, that the intensity of the 1.4-eV emission band may be directly related to defects due to surface damage.

Crystal Structure

CdTe belongs to the II-VI semiconducting compounds. It has a stable crystallographic structure which is characteristic of zinc blende. This structure may be thought of as two face-centered cubic structures displaced from each other by one-fourth of the body diagonal (9), as shown in Figure 1. There are four atoms per primitive cell. Using the indices [uvw] to represent the direction of a vector in the crystal, the vector displacements of the Cd atoms are [000]a, [011]a/2, [101]a/2, and [110]a/2 and those of the Te atoms

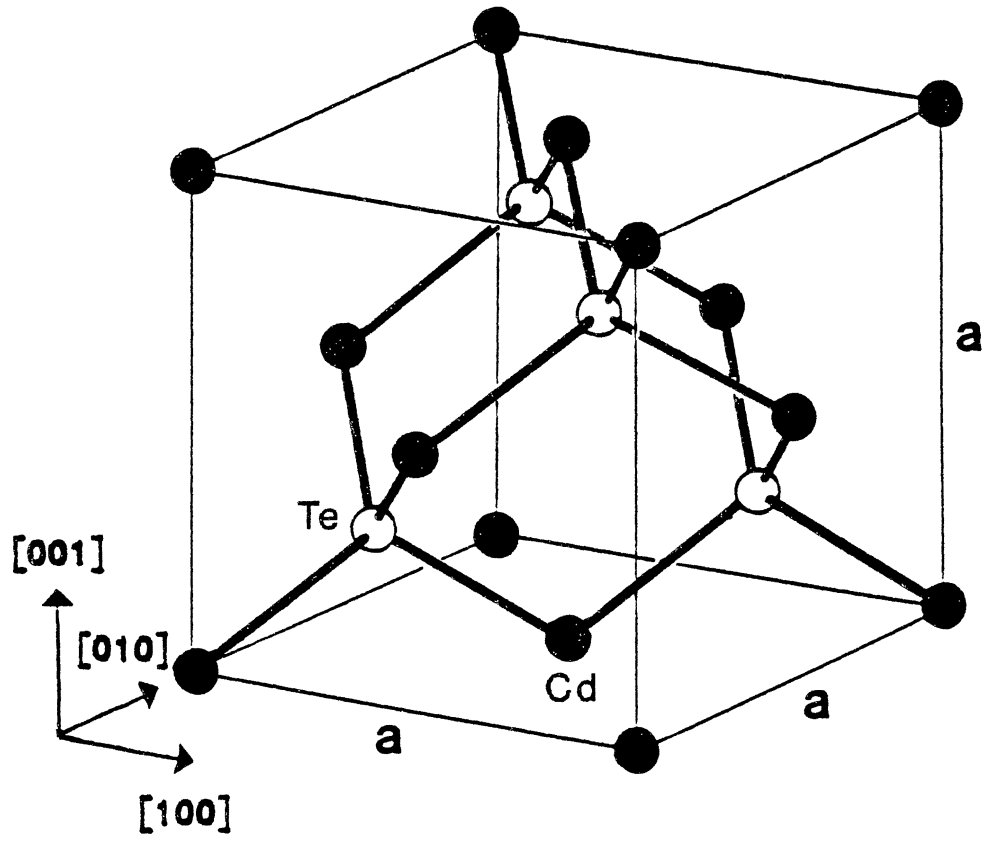

Figure 1. A Unit Cube of the Zincblende Structure in Cadmium Telluride

are [111]a/4, [133]a/4, [313]a/4, and [331]a/4. Thus, the Cd atoms represented by their vector displacements form the corners of a regular tetrahedron that has a Te atom at its center.

The structure may take on a slightly distorted form when doped with a transition metal such as manganese (Mn). This is an element with a partially filled d shell which is stable and strong, and is characteristic of transition metals. The atomic structure of Mn is the Argon-like-$3d^5 4s^2$ structure whereas Cd and Te have the Krypton-like-$4d^{10} 5s^2$ and -$4d^{10} 5s^2 4p^4$ structures, respectively. Since the 2+ configuration of Mn has an ionic radius of about 0.80 Å and that of Cd an ionic radius of 0.97 Å, Mn could substitute on a Cd site. The substitution could give rise to acceptor states since Mn has a lower chemical valency (i.e., the d and s states of Mn have fewer electrons than the d and s states of Cd) than Cd. This kind of defect should not be strictly considered as the only possibility since other types could exist in CdTe. The lattice constant a for bulk CdTe is 6.4829 Å (5).

Scope of this Study

The focus of this study is the 1.4-eV luminescence band. Four experimental techniques have been used to characterize the localized bound states of this emission band in undoped and Mn-doped CdTe samples. The techniques used involve PL, thermal quenching, excitation intensity dependence of PL and time-resolved measurements. PL spectra are obtained from a

.MT 1.0"
variety of samples at 77 K and low temperature (usually between 11 and 16 K). At 77 K, two closely overlapping emission components are normally seen with peak energies at about 1.47 and 1.49 eV. At lower temperatures, however, phonon replicas of these components are seen. By observing the thermal annealing behavior of and by applying Hopfield's relation to the defect band, it is concluded that the components are legitimately two localized bound states. Thermal activation energies of these hole states are obtained with the values of 0.11 and 0.13 eV from the thermal quenching measurements. A set of coupled, first order differential equations are used to predict energy shifts from excitation intensity and time-resolved measurements. The shifts are observed in the experimental data and supported by the theoretical predictions. Finally, a model based on free-electron to trapped-hole recombination is presented to explain the PL data. In addition, mechanisms are proposed for each of the processes observed during thermal quenching.

CHAPTER II

EXPERIMENTAL PROCEDURE

Samples

Single crystals of CdTe used in this study were grown at Eagle-Picher Research Laboratories by a modified Bridgman technique and by a modified Vapor Phase Transport method. The crystals were p-type with high-resistivity close to the order of 10^5 Ω cm. The samples grown by the former method were either nominally undoped or doped with Mn (79 and 400 ppm) whereas for the latter method, the samples were undoped. These materials were mechanically polished to 0.25 microns.

All of the samples used in this work received a cleanup etch for 20 minutes to remove the original surface. The etchants used were either solutions of sulphuric acid and saturated potassium dichromate or bromine in methanol. The concentration for the former solution was 30% by volume of sulphuric acid and 2% by volume of bromine for the latter. Some samples were used for thermally stimulated conductivity (TSC) experiments prior to the photoluminescence experiments. As a result of this, the bromine and methanol solution was used more extensively in order to remove the gold electrodes that were attached to the sample surfaces for the TSC measurements. The dimensions of the samples were 10 mm x 10 mm x

1 mm.

Spectra Correction

In order to correct the data from variations in signal output due to the variable efficiency (as a function of wavelength) of the detecting and measuring devices, a quartz iodine lamp (traceable to NBS) was used as a standard light source. A plot of the standard irradiance curve of this source is shown in Figure 2. A correction curve was generated by dividing the measured irradiance by the standard irradiance (i.e., as measured by NBS). The emission spectra were multiplied by the correction curve to obtain the corrected spectra.

Photoluminescence and Thermal Quenching Spectra

Emission spectra were obtained from photoluminescence and thermal quenching measurements with the experimental setup shown schematically in Figure 3. The sample was cooled to low temperatures by using a CTI-Cryogenics model 22 Cold Head which was part of the model 22C Cryodyne Cryocooler system. The temperature was controlled by a TRI Research T-2000 Cryo Controller and monitored with a Cryo Cal Cryo Diode sensor. For the quenching studies, the temperature ranged from 70 to 110 K. To optimize the luminescence signal, the sample was mounted on the copper cold finger so that the laser beam and a line normal to the surface of the sample

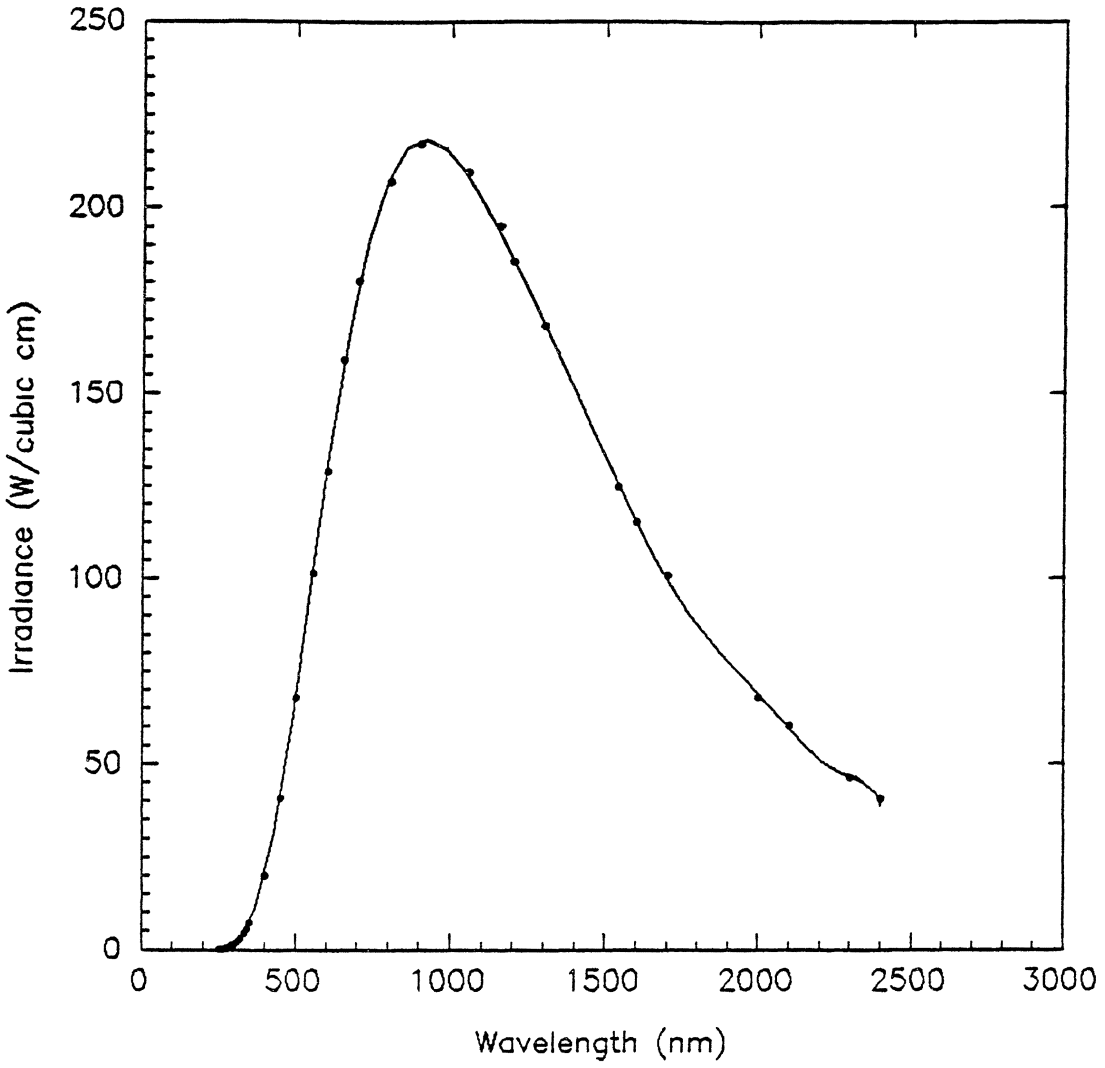

Figure 2. Standard Irradiance Curve of the Quartz-Iodine Source

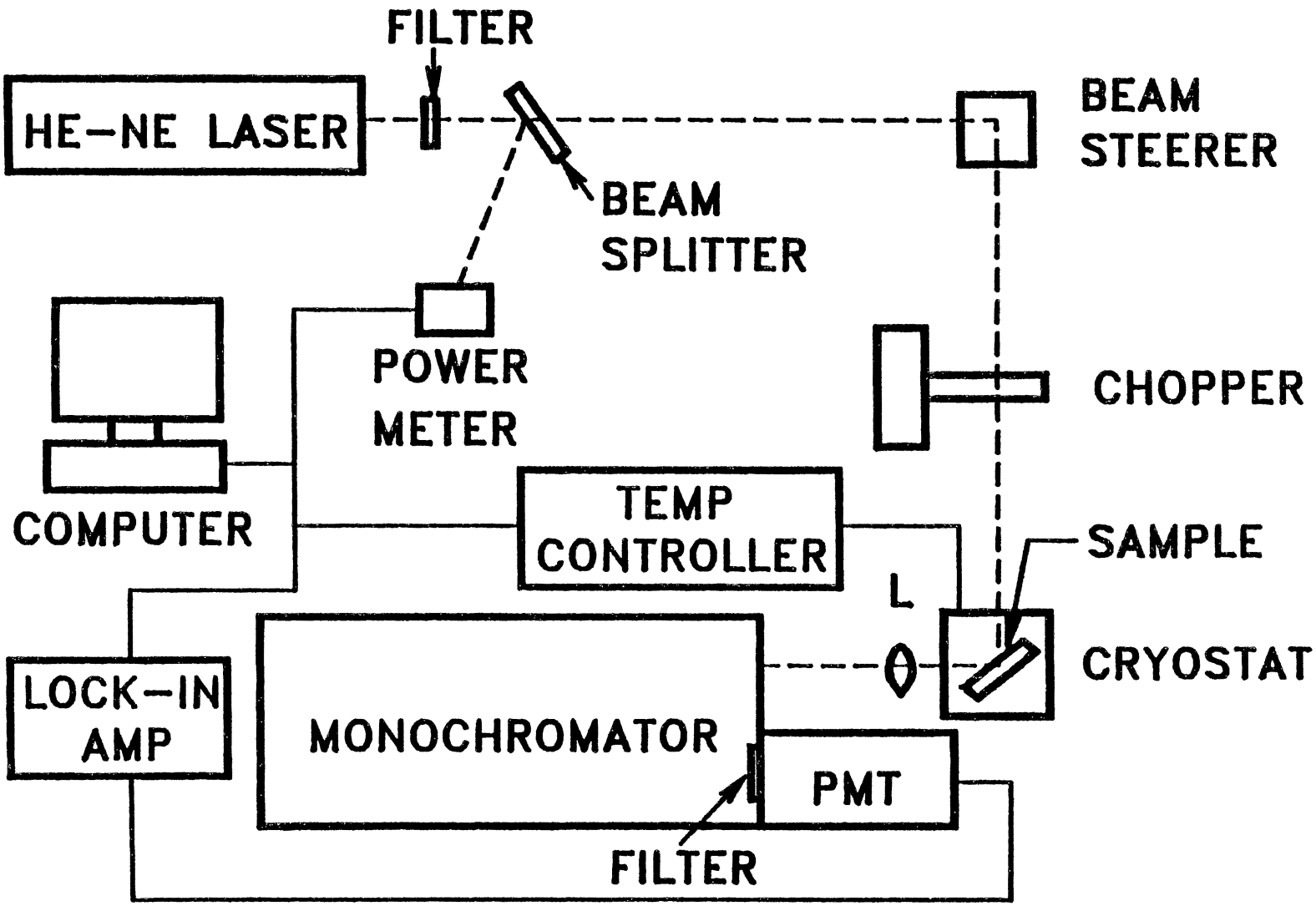

Figure 3. Experimental Apparatus for Photoluminescence and Thermal Quenching Spectra

formed an angle between 45 and 50°. A model ML855 Helium-Neon Laser from Metrologic Instruments served as the excitation source. The beam passed thru a laser line filter to block out unwanted flourescence lines from the lasing medium. To compensate for power fluctuations in the beam, part of it was singled out by a beam splitter with 10% reflection and was monitored with a model 815 Power Meter from Newport Research Corporation. As a result, all measurements were then divided by the output from the power meter to obtain the final spectra.

The luminescence spectra were measured by using a SPEX model 1702/04 Monochromator with focal length of 0.75 m for which a low pass filter was placed at the exit slit to cut off any scattered light in the region of the emission signal. The entrance slit was set as norrow (usually less than 100 μm) as possible with the exit slit twice the size of the entrance slit to get good resolution of the emission lines. A 100 W low-pressure Hg lamp was used for calibrating the monochromator to one-tenth of an Angstrom. The signal was detected with a Thorn EMI Gencom Inc. model 9684 Photomultiplier Tube (PMT) with S-20 spectral response. A chopper was used in conjunction with an Ithaco model 3962 Single Phase Lock-In Amplifier to synchronously detect the signal output from the PMT. Some peripheral devices (shown in the diagram) were interfaced with an HP-86B Microcomputer from Hewlett Packard for data storage and analysis.

A computer code was written to do these experiments. The

code was written in such a way that the wavelength, emission intensity per wavelength, beam power and the qoutient of emission intensity and beam power were recorded. For the quenching studies, it was necessary to maintain each temperature of the sample for one hour and a half so that it would reach thermal equilibrium. The temperature was held constant to within ± 0.1 K.

All measurements were carried out in a vacuum of 10^{-6} torr.

Excitation Intensity Spectra

The experimental setup used for the PL dependence on the excitation intensity is shown in Figure 4. After replacing the He-Ne laser with the Ar-Ion laser, the setup is the same as that shown in Figure 3 except for the addition of a variable beam attenuator (VBA) and a transimpedance amplifier (TIA). The former was a Newport Research Corporation model 935-5 whereas the latter was a circuit built in the lab which comprises a 10 MΩ feedback resistor and an Operational Amplifier model LF357J. Since this circuit had a gain of about 1000, the PMT power supply was set from 1630 to 1260 V for better noise statistics. When the attenuator was not available, spectra were also recorded by using a set of Reynard Enterprises, Inc. Metallic-Coated Neutral Density Filters. The excitation source used in these experiments was the 514.5 nm line from a Spectra-Physics model 2020 Argon-Ion Laser. For this work, the laser beam power ranged from 0.20

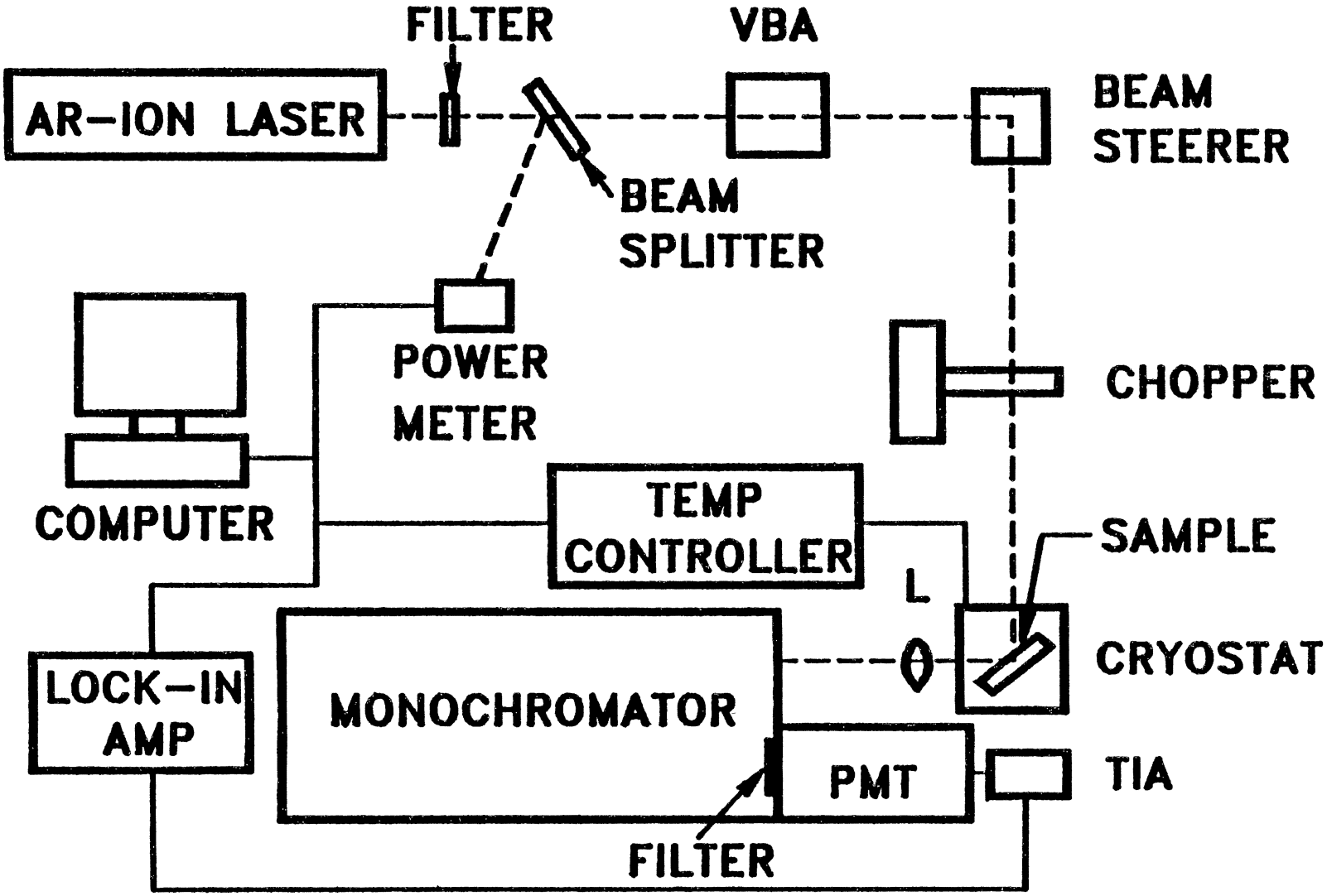

Figure 4. Experimental Apparatus for Excitation Intensity Spectra

to 170 mW. A different PMT was used with S-1 spectral response to improve the sensitivity in the near IR. In order to reduce saturation effects due to laser heating, a CaF_2 disc was placed on top of the sample to serve as a heat sink medium. On top of this plate was a copper plate with a square hole in the center to hold the CaF_2 disc in place. Indium foil was used between the sample and the heat sink disc, and between this disc and the copper plate to provide good thermal contact. Refer to Figure 5 for a schematic representation of this arrangement. Basically, this experiment consisted of changing the laser beam power and recording the change in PL spectrum. The beam power was changed by using the attenuator or filters of different optical density. Since the emission signal was amplified by the TIA, the entrance slit was normally set to 50 μm. This corresponded to a resolution of 1.1 Å.

It should be noted that the heat sink disc was found to work since the luminescence signal was observed to increase to a larger extent in proportion to the larger power range applied to the sample. This was necessary to do considering that before using the disc, the signal would increase as the power increased but then it would decrease with increasing power due to saturation of the luminescence signal.

Time-Resolved Spectra

The experimental setup for these measurements is shown in Figure 6. The excitation source was a Xenon Corporation

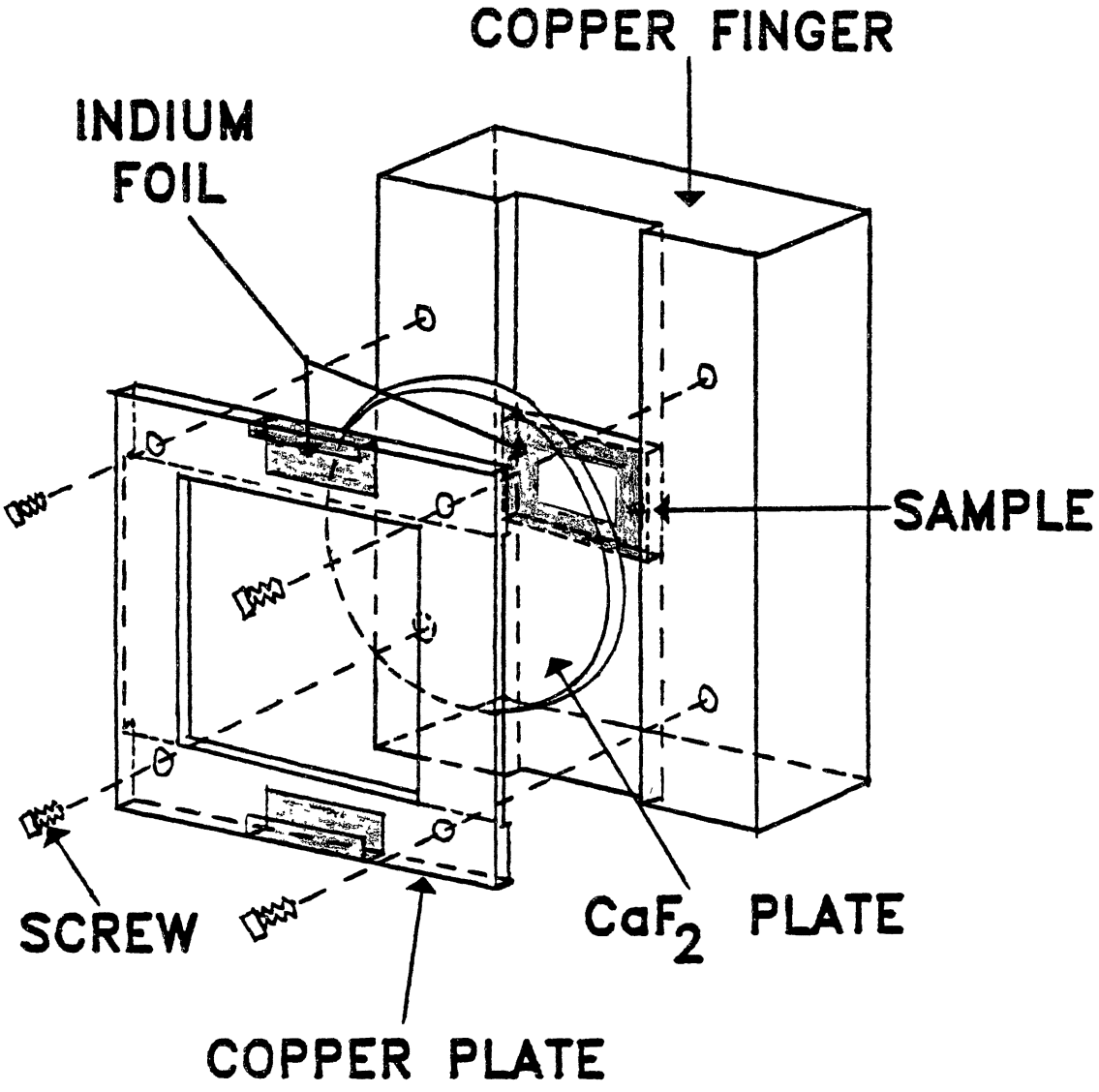

Figure 5. Copper Block Arrangement for Holding the Samples in Place

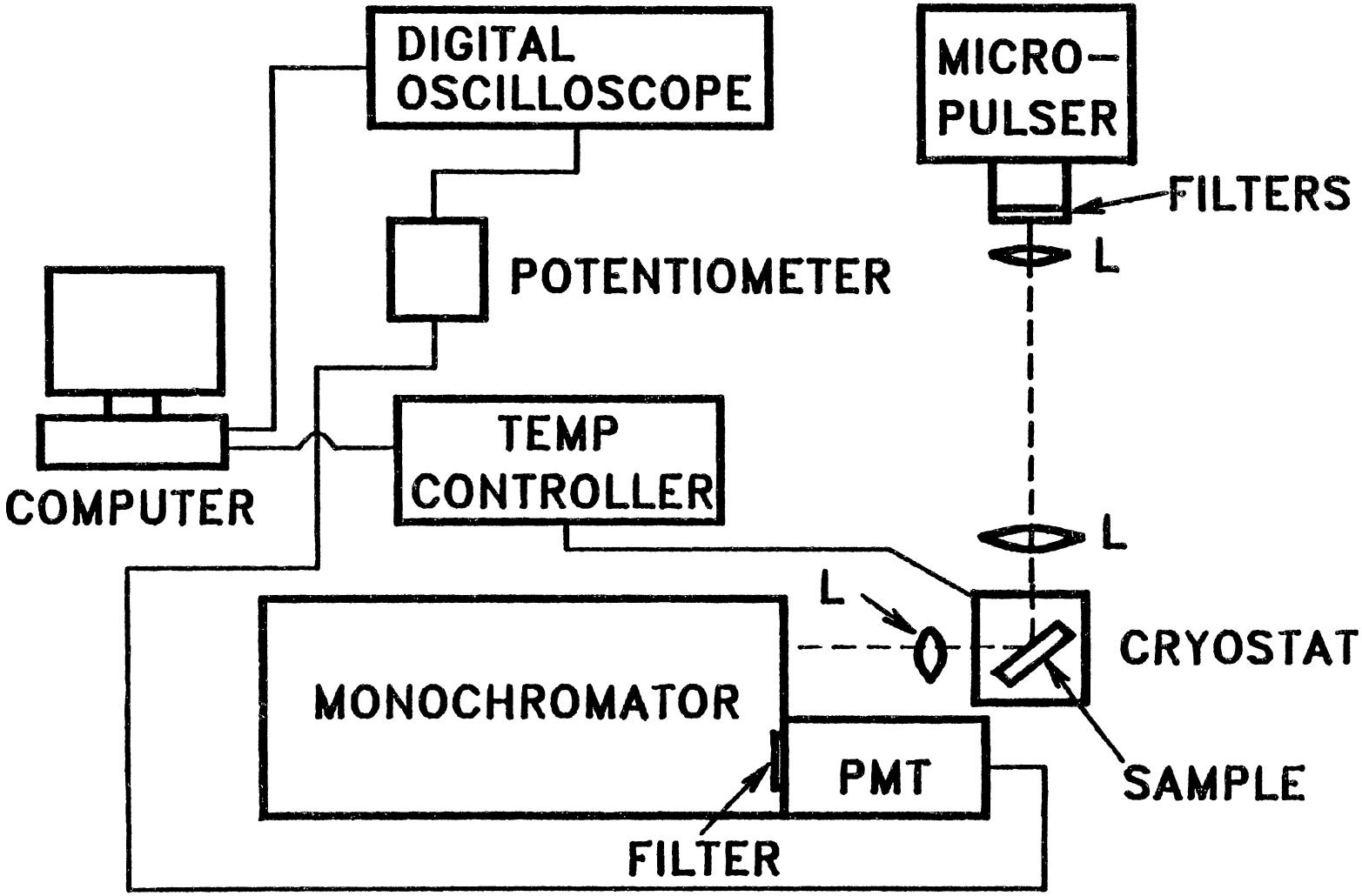

Figure 6. Exprimental Apparatus for Time-Resolved Spectra

model 457A Micropulser with a pulse width of 2.5 μs and a variable repitition rate of about 2 Hz. A point source flash tube with Xenon as the ionizing gas was used by discharging the capacitor to 8.5 kV. The unit was designed to deliver 1 to 10 Joules of energy per pulse with a variable voltage adjustment from 2 to 10 kV. The voltage setting used was 8.5 kV in order to keep radio frequency (rf) interference to a minimum. Also, a Faraday cage was constucted from a brass wired-mesh material to suppress rf noise (18). To suppress rf noise even further, the power supply was placed in another room and the high voltage cables were twisted and shielded with rigid wall conduit to eliminate electromagnetic induction. Furthermore, the signal source cables were shielded with a thick wired-mesh material and the chasis ground of the power supply was mantained floating with respect to an electrical ground to eliminate ground loops. Three wide bandpass filters were used in tandem to block out UV and IR light. The luminescence signal was measured and detected by the monochromator and PMT, respectively. These devices were described earlier. Again, the samples were mounted in the same manner as described before from the previous experimental setup. A LeCroy model 9400A Dual 175 MHz Digital Oscilloscope was used to capture the signal transients. To pick up the signals in real time, a potentiometer was built for impedance matching.

The experiment consisted of exciting the sample with a pulse of light and then recording the luminescence waveform in single shot mode. Once the waveform was frozen in the

oscilloscope, a set of data points from the waveform was extracted according to specific decay times chosen (i.e., 0, 1, 2, 4, 6, 10 and 15 μs were chosen) from a computer program that was written. The set of points was selected 20 times and the average was taken for each point. This was done to average out noise.

CHAPTER III

PHOTOLUMINESCENCE AND THERMAL QUENCHING SPECTRA

Introduction

This chapter will deal with PL spectra taken at 77 K and 12 K, primarily from samples grown from the melt. Data on thermal quenching of the PL spectra will also be presented from these materials. The differences in the overall PL emission between etched and unetched sample are pointed out. The data indicate that the 1.4-eV broad emission band is made up of at least two overlapping components. From a study of the temperature dependence of this emission band, activation energies are calculated for the two emission components using an Arrhenius plot. The 1.4-eV emission bands are compared for samples grown from the melt using the Bridgeman method, and by Eagle-Picher's modified vapor phase transport method. Finally, a model is proposed to explain the PL and thermal quenching results.

Experimental Results

Figure 7 shows a typical PL spectrum taken at 77 K from CdTe and illustrates the main features of interest. The spectrum was obtained from a Mn-doped (79 ppm) sample and

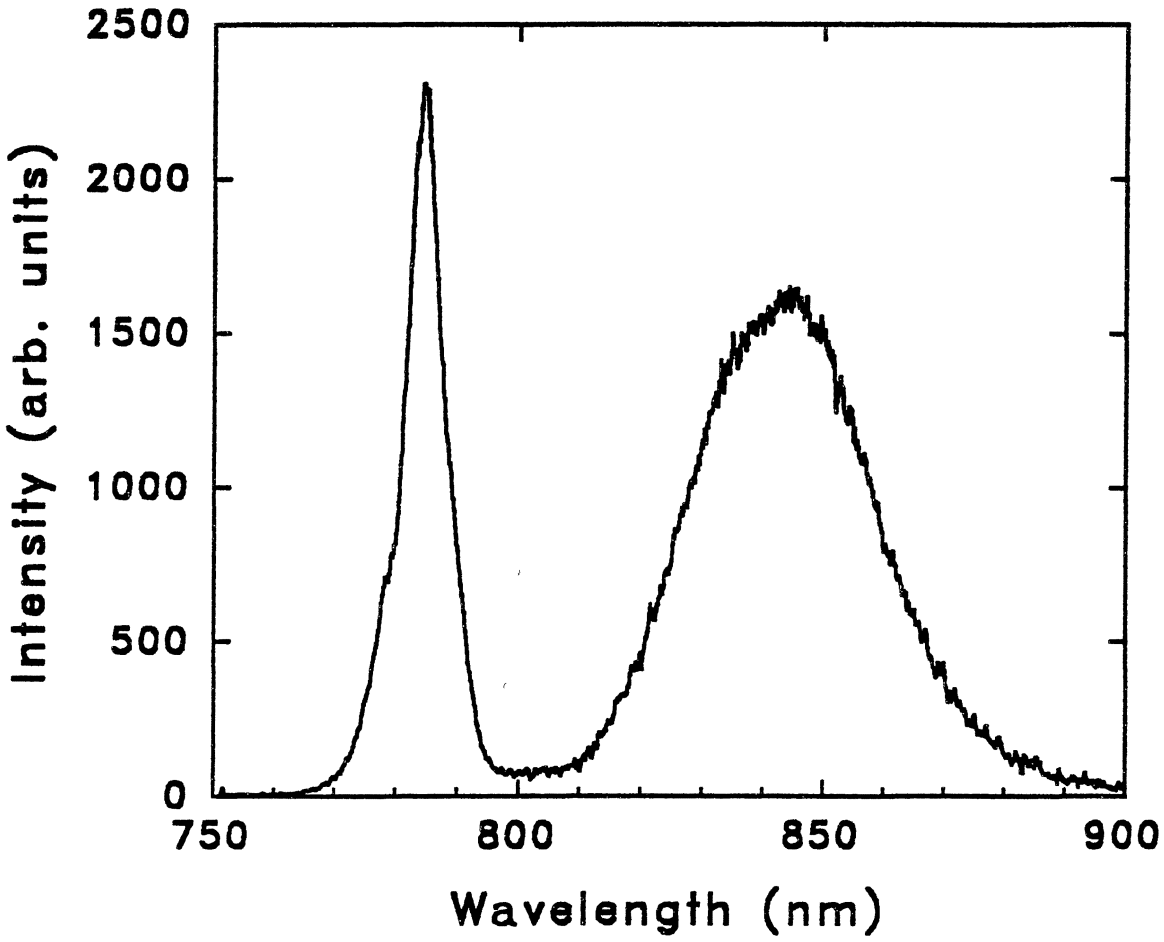

Figure 7. PL Spectrum at 77 K from a Mn-Doped (79 ppm) CdTe Sample

shows the narrow band near 1.58 eV (785 nm) due to free- and bound-exciton emission and the broad-emission band near 1.47 eV (843 nm). All of the melt grown samples used in this study exhibited these general emission characteristics. As stated in Chapter I, the energy of the broad emission band is highly variable from sample to sample and despite the fact that in this sample the band is near 1.47 eV, the usual description of 1.4-eV emission band will be used throughout this thesis.

It is worthwhile to point out that the luminescence intensities of the 1.58 and 1.4-eV emission bands varied considerably under different conditions. For example, the luminescence intensities and shapes of the bands depended upon the particular sample used. For most samples, the 1.4-eV emission normally showed two emission components whereas only one component was seen in some other samples. It is reported elsewhere (15), and is generally observed, that as the impurity content increases, the 1.4-eV emission band becomes broader, occasionally showing more than one emission component. However, this was not the case from the results obtained in this study since it was found that some pure samples also revealed more than one emission component. As another example, it was noted when the laser beam was changed to a different spot on the sample, both the overall and the relative luminescence intensities of the 1.58- and 1.4-eV emission bands were affected dramatically. To reduce this effect and to ensure as much reproducibility of the PL spectra as possible, all the samples received a "clean-up" etch.

After the samples were etched, the relative variability between intensities of the emission bands was still present but was less noticeable. It was also noted that the luminescence intensity was more variable for the unetched samples than for the etched samples.

The differences in PL spectra between an undoped, etched and unetched sample are shown in Figure 8. For the unetched case, it is readily apparent that two emission components are seen in the broad-emission band with one component near 1.47 eV and the other near 1.49 eV. It is noted that most of the luminescence intensity is due to the 1.4-eV emission band which is more prominent than the 1.58-eV band. For the etched case, most of the luminescence intensity is due to the exciton band, and the two components in the broad-emission band are seen but are not as apparent as in the unetched case. It was also found that the overall intensities actually increased after etching when the intensity scales were compared from both spectra.

In view of the observations noted above, it is clearly seen that some sort of relationship exists between the 1.4-eV emission band and surface defects caused by mechanical polishing. This is in general support of the suggestion previously made by Myers et al. (13). According to these authors, they were able to vary the luminescence intensity by changing the method of surface polishing. For example; from the mechanical, chemimechanical and hydroplaned polishing techniques employed in their work, the relative intensities of

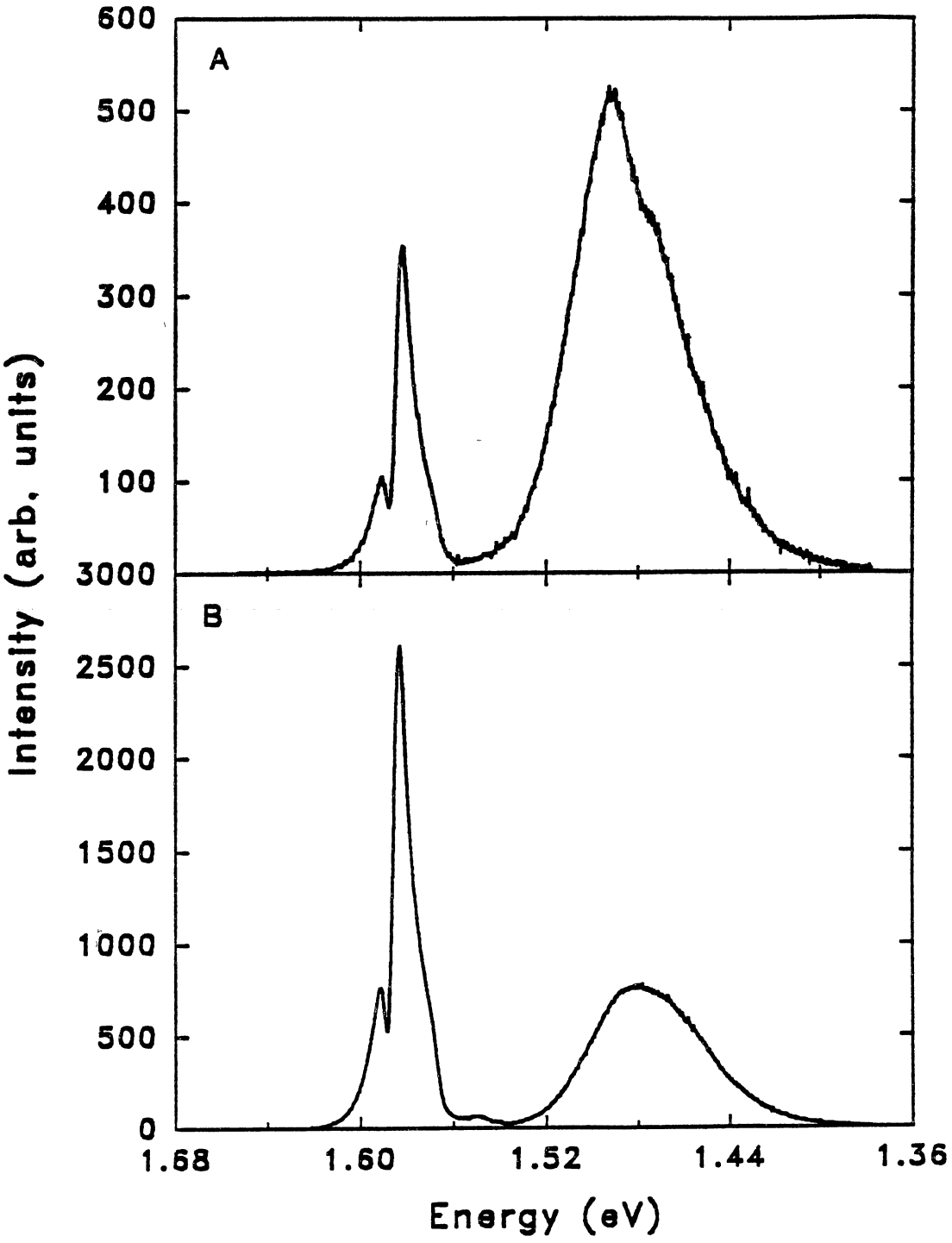

Figure 8. Effects of Etching on the PL Signal from an Undoped CdTe Sample

the 1.58-eV and 1.4-eV emission bands as well as the overall luminescence intensity changed as a function of the surface polishing method. Furthermore, they observed that the relative intensity of the two bands and the overall luminescence intensity varied substantially from sample to sample. This luminescence behavior is also seen in the present study. As pointed out by Zanio (9), and Agrinskaya et al. (11), the intensity of the 1.4-eV emission band is definitely related to impurity-doping in CdTe. However, as noted by Myers et al. (13), not only is the intensity of this emission band affected by impurities but is also affected by surface defects. As a consequence, the present study does not necessarily declare, as do Myers et al., that the 1.4-eV emission band is directly related to surface defects. It is thought instead that the observed variability in the luminescence intensity seen from etched to unetched sample, from sample to sample and from one spot location of the laser beam to another spot location on the same sample may be due, at least in part, to competing processes caused by presence of surface-damage states. This will be shown later in the chapter.

It should be mentioned that a study was conducted to determine if the strength of the overall luminescence signal is affected by the repeated use of the etching solution. It was found that the luminescence intensity increased each time after the sample was etched in 5-minute intervals, and reached a steady intensity value at the fourth interval. That is, after 20 minutes the overall emission intensity remained

constant. As a result, all of the samples used in this study were etched for 20 minutes to get a maximum signal output from each sample.

Figure 9 shows some PL spectra as a function of temperature in the 1.4-eV emission region. The presence of the overlapping emission components is clearly seen again, with one component near 1.47 eV and the other near 1.49 eV. As the temperature is raised, an apparent shift in peak maximum is observed to occur from higher to lower energies. A possible cause of this shift in energy, is the change of the bandgap energy of the material. The bandgap energy of CdTe is 1.607 eV at 0 K and 1.44 eV at 300 K (19). Thus, the difference in energy is 0.167 eV from 0 to 300 K. Since the temperature range of the present experiments is only from 70 to 90 K, it may be safely presumed that no appreciable energy shifts due to this effect occur in Figure 9 and these can thus be ignored. From Figure 9, it should be noted that although the the LO phonon energy in CdTe is 0.02 eV, which is equal to the difference in energy of the two components (viz., 1.47 eV and 1.49 eV), this does not mean that the two components are phonon replicas of each other since the two signals show different annealing rates. It is this difference in annealing rates that causes the apparent shift in energy of the 1.4-eV emission band as the temperature is varied.

The Arrhenius plot shown in Figure 10 illustrates the thermal quenching characteristics of the 1.47 and 1.49 eV emission components. The two curves resulted from attempts

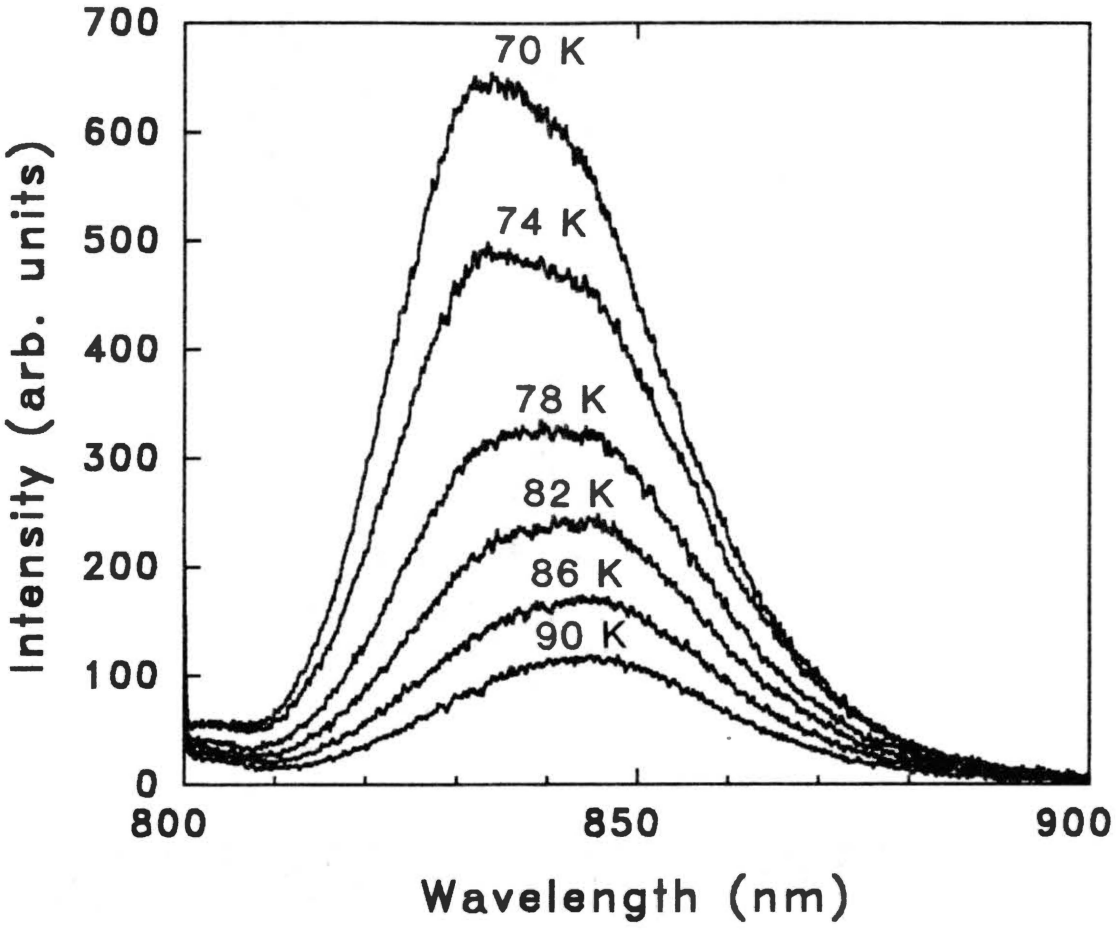

Figure 9. Thermal Quenching Spectra of the 1.4-eV Emission from the Sample in Fig. 8

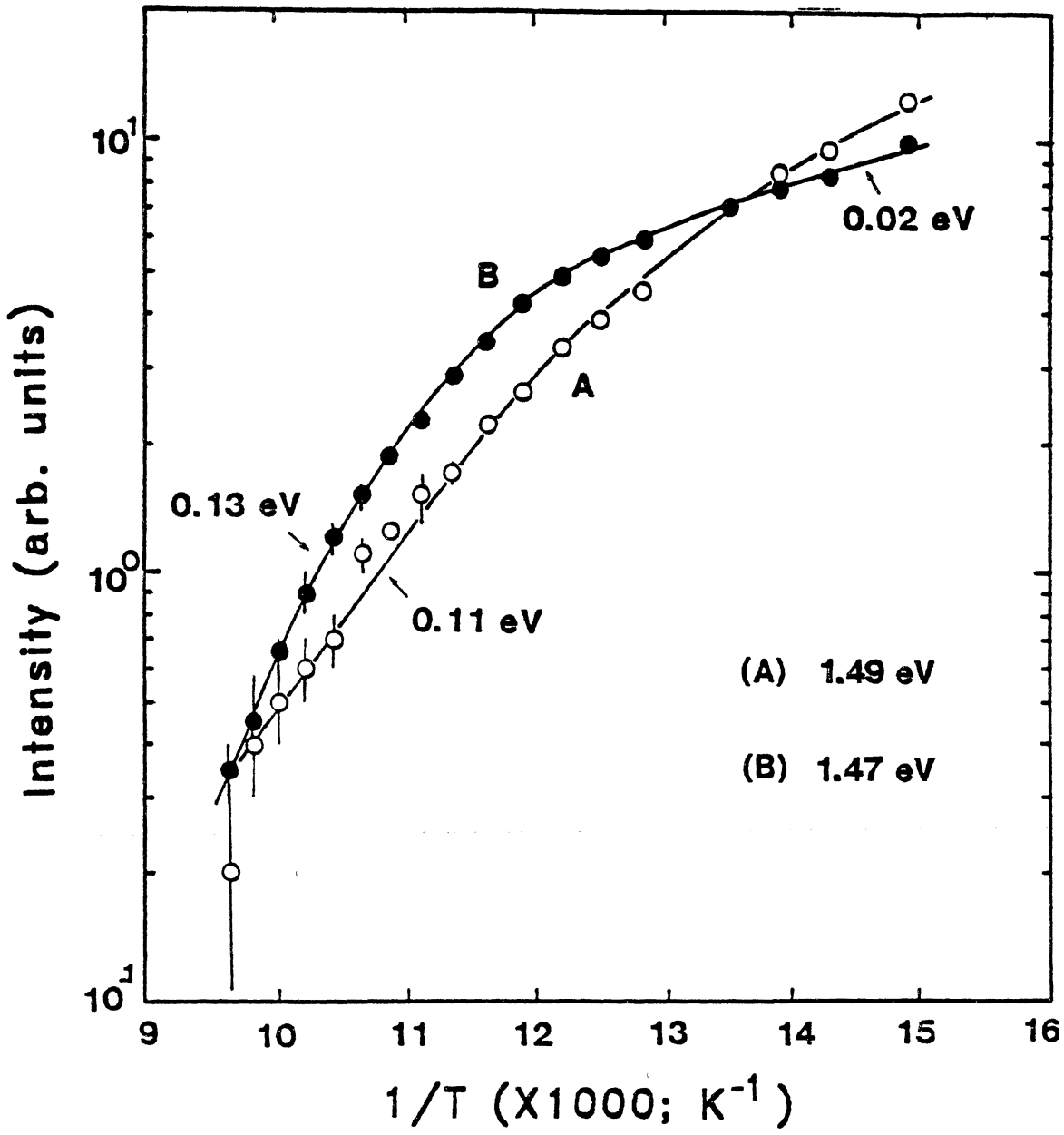

Figure 10. Arrhenius Plot of the PL Thermal Quencing Data from a Mn-Doped (79 ppm) CdTe Sample

to separate the thermal quenching characteristics of each overlapping peak shown in Figure 9 by selecting two different wavelengths. Curve A was generated by measuring the intensity of each spectrum at 825 nm. This wavelength was chosen so that the intensities from the trailing edge of the 1.49-eV peak would be sampled more than that of the 1.47-eV peak. In the same manner, curve B was generated by measuring the intensity at 855 nm.

The activation energies for thermal quenching were obtained using the Arrhenius law (20), namely:

$$I(T) = \text{constant} \times \exp(-E/kT). \qquad (3.1)$$

Here E is the activation energy and k is Boltzmann's constant. Thus, from the straight line portion of the plot, the slope can be obtained and set equal to -E/k. From Figure 10, and using the above equation, an activation energy was calculated from curve A with a value of 0.11 eV. The two activation energies of 0.02 and 0.13 eV from curve B were obtained in the same fashion. The accuracy of the activation energies from the plot are limited by experimental errors, as shown by the error bars. However, the experiment was repeated many times on different samples. The values calculated from these other samples were within ± 3 meV of the values just presented, so it is believed that the errors generated are relatively small. The thermal quenching spectra were not analyzed by using a deconvolution routine due to the fact that a summation of Gaussians would have had to be fitted using a con-

stant energy bandwidth -- a difficult thing to do since the data were taken with a constant wavelength bandwidth.

As mentioned earlier, the presence of two overlapping emission components is seen in most samples whereas in the others, only one component is observed. As a result, for those specimens which displayed the 1.47 and 1.49 eV components, it was found that each one quenched with activation energies of 0.02 and 0.13 eV for the former peak and 0.11 eV for the latter. When only the 1.47 eV component was present, it was found to quench with a single activation energy of 0.13 eV. The 0.02 eV process was absent. It is interesting to note that the quenching results of Agrinskaya et al. (11) show such a process but no mention was made of this throughout the discussion in that paper. Furthermore, other authors seem to ignore this process despite the fact that the asymmetric shape of the 1.4-eV emission suggests the presence of more than one emission component (16,17).

Discussion

To further support the argument that the 1.47 and 1.49 eV emission peaks are not phonon replicas of each other is made by the PL spectrum taken at 12 K in Figure 11. This figure shows the phonon structure (these peaks could be other defect-related components) of the 1.4-eV emission with the peaks of interest, labeled by I_a, I_b, I_c, and I_d which correspond to energies (from I_a to I_d) of 1.4975, 1.4760, 1.4565 and 1.4354 eV. Starting with I_a, the energy separation be-

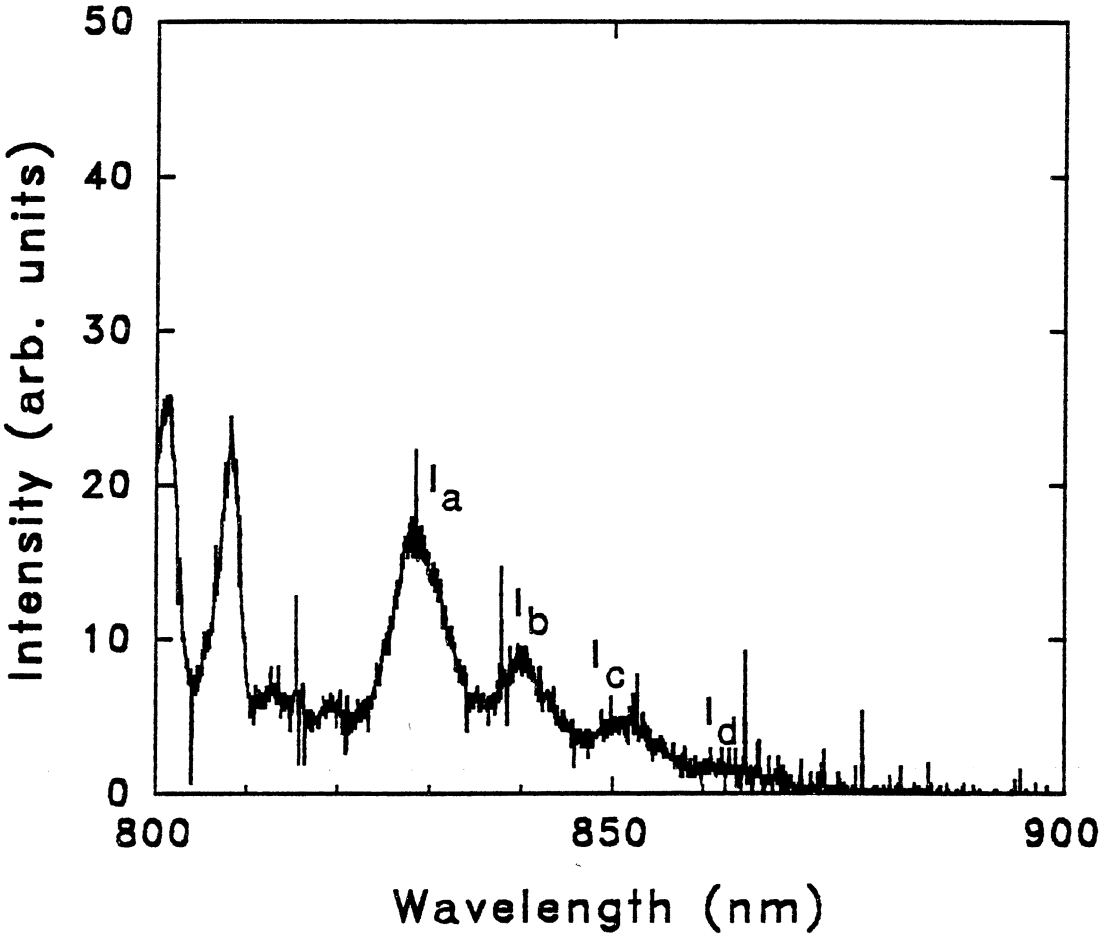

Figure 11. PL Spectrum at 12 K of the 1.4-eV Emission from an Undoped CdTe Sample

tween adjacent peaks is approximately 21.5, 19.5 and 21.1 meV. Although these energies are close to the LO phonon energy (21.3 meV) in CdTe, the distinction between phonon and defect-related peaks remains to be determined. This is described below.

An elegant theory was developed by Hopfield (22) to describe the relative intensity of the individual peaks shown in Figure 11. This theory only applies to localized bound states, and is strictly used in the absence of thermal optical phonons. Thus, since only LO phonon emission is presumed (because of the energy separation between each component), the relative intensity of each peak is given by

$$I_n = I_o \frac{\bar{N}^n}{n!} \qquad (3.2)$$

where I_n is the intensity of the nth phonon emitted peak, I_o is the intensity of the zero-phonon peak, and $\bar{N}$ is the average number of phonons emitted during an electron transition. Straightforward application of Equation (3.2) shows that if I_a is the zero-phonon peak, then the relative intensities I_b/I_a, I_c/I_a and I_d/I_a do not agree with this equation. If I_b is the zero-phonon peak, then the ratios I_c/I_b and I_d/I_b do agree with Equation (3.2) to a large extent. Thus, I_b is the zero-phonon peak with peaks I_c and I_d as the first (1LO) and second (2LO) phonon replicas, respectively. Apparently, peak I_a has no phonon emission and could be considered as the other defect-related peak. It should be noted that at 12 K, the energies of I_a and I_b are 1.4975 and 1.4760 eV, respec-

tively. At 77 K, these peaks will shift to lower energy as a result of the change in the bandgap. Most of the samples studied revealed the same conclusions, i.e., that peaks I_a and I_b are the two defect-related emission components with I_c and I_d as phonon replicas.

As mentioned previously, the foregoing argument strictly applies to individual phonon peaks, and it should be noted that the ratios I_c/I_b and I_d/I_b do not agree exactly with Hopfield's relation since there may be underlying emission components which would upset the measured ratios. It should be noted also that according to Hopfield's theory (22), it is highly improbable for the recombination of a hole in state k and an electron in state k' to occur with the emission of no phonons, which seems to be the case with peak I_a. However, it may be possible that the phonon replicas of I_a and I_b are strongly overlapping thus giving the apparent emission of no phonon lines for peak I_a.

In Figure 7 was shown a PL spectrum at 77 K from an undoped CdTe sample. It was pointed out that the 1.58 and 1.4-eV emission bands were characteristic of all the melt grown samples studied. Samples grown by the modified vapor phase transport method were also studied in this work. The vapor phase transport method was developed some years ago and has been used to improve the crystal growth quality of CdTe. However, Eagle-Picher Research laboratories modified this method to further refine the quality of these crystals.

Figure 12 shows a PL spectrum at 77 K from an undoped

CdTe sample grown by the modified vapor phase transport method. It is interesting to note that this figure reveals the same spectral features as those seen from the PL spectra of the melt grown materials. That is, the 1.58- and 1.4-eV emission regions are observed in these materials even though there is a slight difference in the shape of the 1.4-eV luminescence band. From Figure 12, the position of the peak maximum of the broad-emission band is near 1.49 eV with an overlapping component near 1.47 eV. Unlike most of the melt grown samples studied, the broad-emission band showed two weak emission components, one on each side of the band. Another feature noted in all the vapor phase samples is that the overall PL intensity at 77 K was usually weak. The PL emission of these samples was also unusual in that the shape of the 1.4-eV emission band critically depended on the etching solution used. In one instance, when a sample was etched in the bromine-methanol solution, the 1.4-eV luminescence band was absent and the exciton band exhibited two weak emission components on its low energy side. There were other instances where the 1.4-eV luminescence band exhibited strong phonon structure when the sulphuric acid and saturated potassium dichromate solution was used. This was unlike other samples etched in the sulphuric acid solution where the 1.4-eV band showed little phonon structure. In spite of this, most of the vapor phase samples showed the two overlapping emission components in the 1.4-eV band.

Many thermal quenching studies on the 1.4-eV lumines-

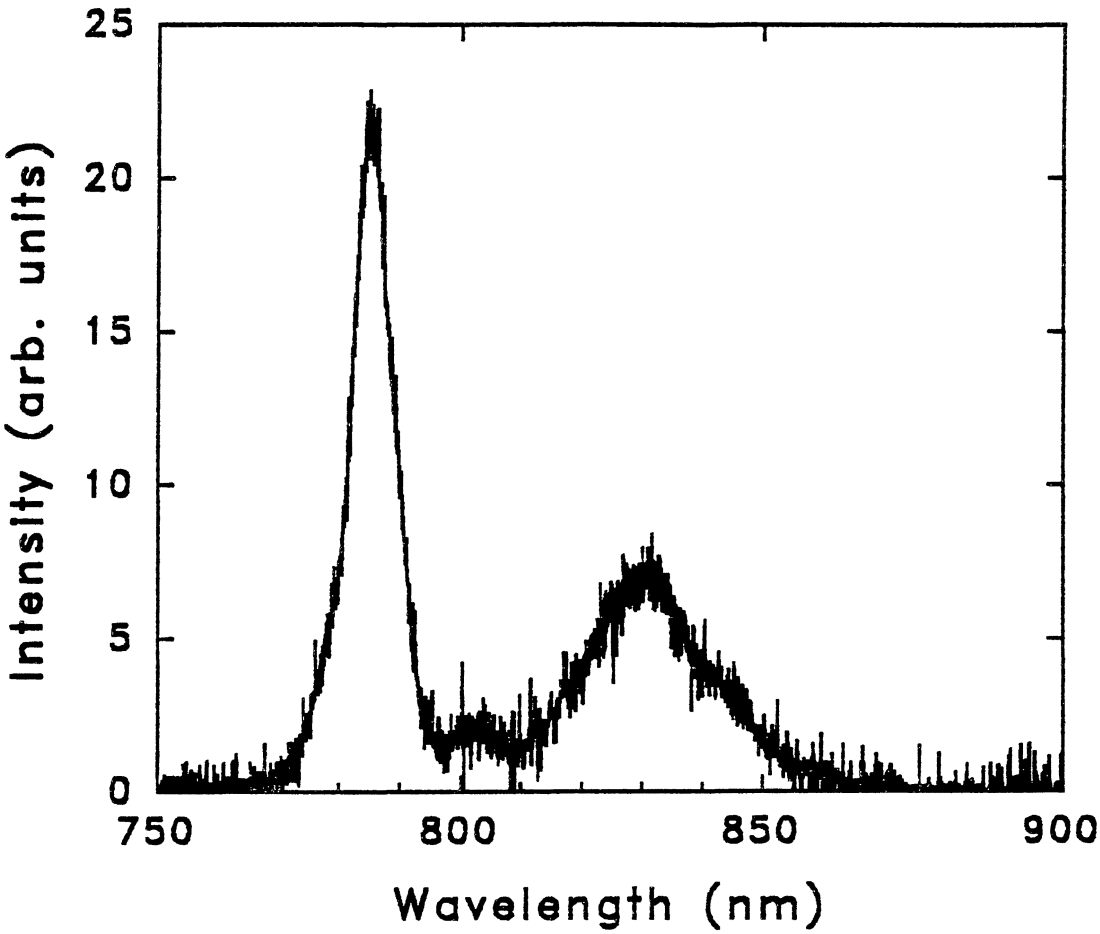

Figure 12. PL Spectrum at 77 K from a Sample Grown by the Vapor Phase Transport

cence band have been reported in the published literature where it has been suggested that the thermal quenching process is due to the thermal release of trapped holes from a hole state to the valence band (9,12). Thermally Stimulated Conductivity (TSC) results clearly support this evidence. From TSC experiments (19), a TSC peak is observed during thermal quenching and is due to the thermal release of trapped holes. It is worth stressing that the activation energy obtained from TSC measurements is 0.13 eV and agrees well with that observed during thermal quenching.

It is noted that the 0.02 eV activation energy observed during thermal quenching has been interpreted elsewhere (8,11,14) as being due to a transition from a bound state below the conduction band (or above the valence band) to the delocalized band. The present study shows that this energy corresponds to the difference in energy of the two overlapping emission components seen in the 1.4-eV emission region, and when only the 1.47-eV emission component is observed, the 0.02-eV process is absent. Hence, if the 0.02 eV process does correspond to a transition from a bound state to a delocalized band, then it must be characterized by a very small probability term in order for this process to occur at temperatures between 70 and 80 K (this will be shown shortly). In view of this, the 0.02 eV process is believed to have the characteristics of an interlevel transition.

The following model is proposed to explain the thermal quenching and PL results, as shown in Figure 13. In this

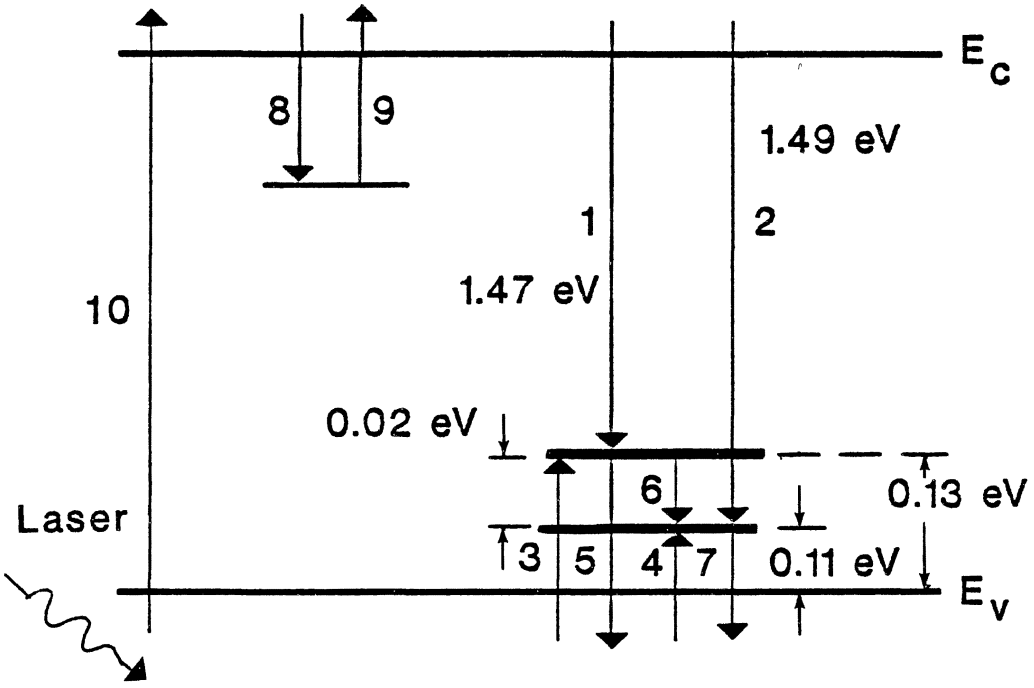

Figure 13. Energy Level Model to Explain the PL Data

model, the luminescence signals are due to transitions of free electrons from the conduction band (transitions 1 and 2) recombining with holes trapped at two hole states (transitions 3 and 4). These hole states are at E_v+0.13 eV and E_v+0.11 eV with emission energies of 1.47 and 1.49 eV, respectively. The thermal quenching processes are indicated by transitions 5 and 7 for the 1.47 and 1.49 eV emission components, and by transition 6 for the interlevel hole process which is due to the thermal release of a hole from the deeper hole state to the shallower state. It should be mentioned that TSC is observed during transitions 5 and 7 but no TSC is observed during transition 6 (19). The electron level below the conduction band is included in the model for charge neutrality with transitions 8 and 9 included for completeness. Transition 10 is the generation of free electrons and holes by the excitation source.

In TSC measurements on these samples (19), it was observed that the TSC signal centered near 103 K in the unetched sample completely disappeared after the sample was etched. This was noted to be suggestive of surface damage states due to mechanical polishing with the defects being removed after etching. Also, another sign of surface-related defects was detected when measurements of the growth of the 103 K peak with illumination time for positive and negative biases were conducted. Furthermore, it was observed that when a negative bias was applied to the illuminated electrode, the TSC spectra were always slightly larger than those when the

positive bias was applied to the illuminated electrode (19). This was suggestive of electron-related defects.

As a result of the observations made above from reference (19), there appears to be some suggestion that the 103 K peak is due to electron release from surface defects. From Figure 13, an electron state has been incorporated in the model to account for all the electron traps. These states are due to trapping and detrapping of electrons due to surface-damage states caused by mechanical polishing. The trap depth of this electron state is at E_c-0.21 eV and was determined from trap depth analysis using peak fitting routines.

The model clearly shows that the traffic of charge of the two hole states is reduced by the presence of the electron traps due to surface-damage states. These traps introduce alternate competing pathways for the elctrons thereby decreasing the 1.4-eV luminescence efficiency. When the surface-damage states are etched away, the electron traps are removed and the 1.4-eV luminescence efficiency increases. This was the case shown in Figure 8 where the overall luminescence intensity increased after etching the samples for this study.

Another point worthy of note is that the interlevel process of 0.02 eV is consistent with calculated transition probabilities (i.e., frequency factors). For example, a transition from a localized level to a delocalized band is characterized by a probability per unit time of the form $(s)x(\exp(-E/k_BT))$, where E is the trap depth, T is the tem-

perature, and k_B is the Boltzmann's constant. In this expression s is a constant involving the attempt to escape frequency and the change in entropy associated with the transition. For the localized level to the delocalized band transitions, s is expected to be of the order of 10^{12}-10^{14} s^{-1}, (21). Thus, s would have to be extremely small for the interlevel transition to occur. By assuming a first-order process, it is estimated that in the present study s is of the order of 10^{5}-10^{6} s^{-1} -- i.e., many orders of magnitude below expected values. However, such small preexponential factors can be characteristic of interlevel, localized transitions wherein the freed charge does not enter the delocalized band. In this situation, the attempt to escape frequency is modified by a factor of p which takes into account the probability of finding an empty neighboring level close enough for the transition to occur. This probability may be very small and, in that case, the resulting preexponential factor (i.e., sp, not s) would also be very small.

CHAPTER IV

EXCITATION INTENSITY AND TIME-RESOLVED SPECTRA

Introduction

Excitation intensity dependence and time-resolved spectroscopy measurements are presented in this chapter. First, it is shown that a shift in energy of the 1.4-eV band is seen to occur from lower energy to higher energy as the excitation power increases. A sublinear power dependence on the 1.4-eV band is also observed. Then, it is noted in time-resolved measurements that a shift in energy occurs from higher energy to lower energy with time after the end of the excitation pulse. A time constant is estimated for the 1.47- and 1.49-eV emission components from these experiments. Finally, it is shown that the above measurements are in support of the model proposed in Chapter III. That is, these observations are predicted based on a set of coupled, first-order, differential equations that were formulated to simulate the traffic of charge between the energy levels shown in the model devised to explain the PL and thermal quenching results.

Experimental Results and Discussion

Figure 14 shows PL spectra at 77 K that were obtained by

varying the intensity of the incident laser beam. The powers shown in the figure were measured at the window of the cryostat and the sample used was a 400 ppm Mn-doped sample. (These and subsequent spectra were recorded with an S-1 PMT to improve the spectral sensitivity in the near IR.) As a consequence of improving the PMT sensitivity, a new feature is apparent in these spectra. The peak maximum is now near 1.45 eV despite the fact that the previous positions of the peak maxima were at 1.47 and 1.49 eV. It should be noted that these two emission components are still present on the high energy side of the broad-emission band. These features were observed in all of the excitation intensity dependence measurements.

In addition to the new features mentioned above, it is interesting to note that more emission peaks become visible in the 1.4-eV luminescence band at higher excitation powers. It is interesting to note also that an apparent shift in energy of the overall emission band occurs from lower energies to higher energies as the excitation power is raised. This shift takes place from 1.43 eV (865 nm) at 1.3 mW to 1.45 eV (858 nm) at 156 mW. The overlapping emission components and the shift in energy were characteristic of the other excitation intensity dependence measurements obtained from the 79 ppm of Mn and undoped samples.

It is worth mentioning that the shift in energy is in support of the observations made by Norris and Barnes, (12), from cathodoluminescence (injection level dependence measure-

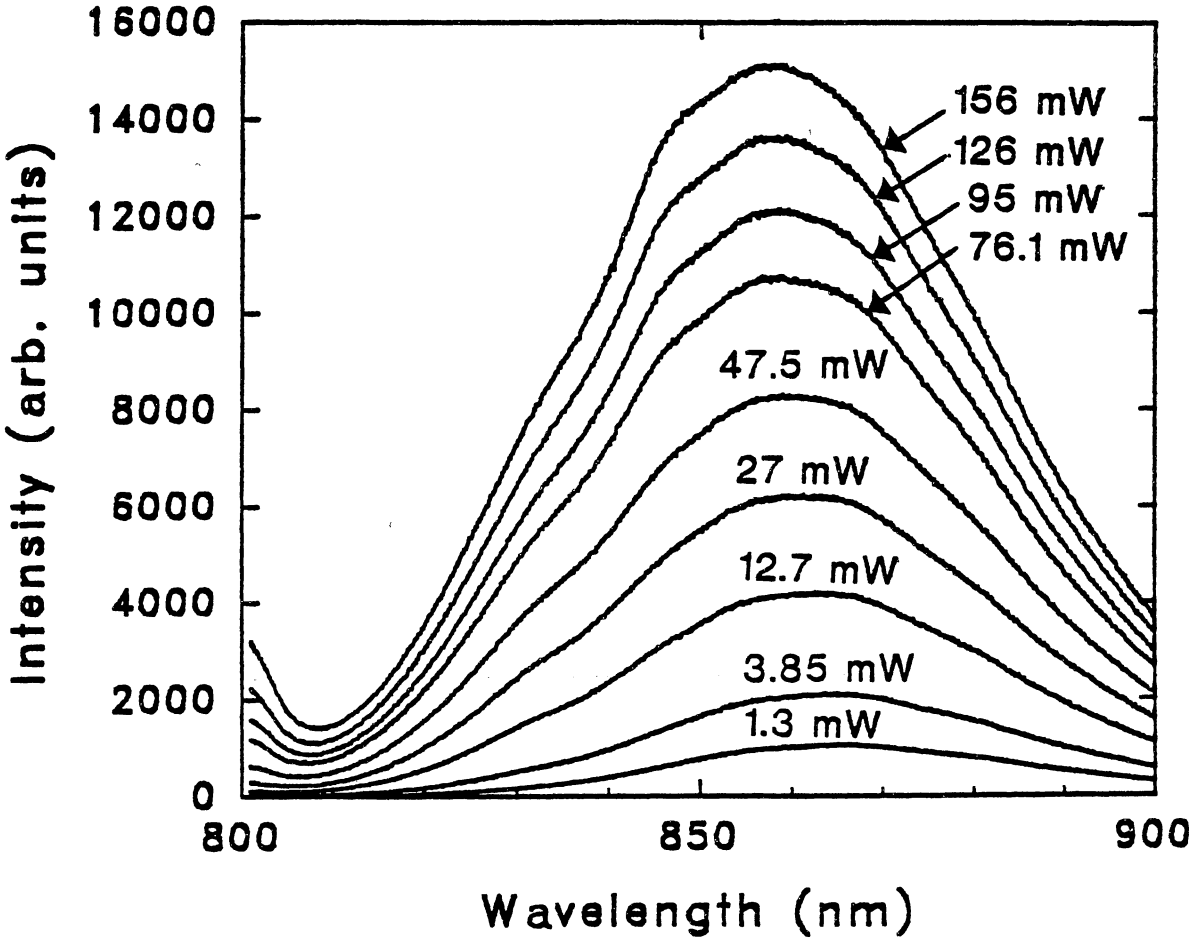

Figure 14. Excitation Intensity Spectra at 77 K from a Mn-Doped (400 ppm) CdTe Sample

ments) experiments. They noted that as the injection level increased, the resulting shift in energy may have been caused by overlapping peaks.

The behavior of the 1.4-eV luminescence intensities as a function of excitation power (from here onward, this will be denoted as f) from the Mn-doped sample in Figure 14 and an undoped sample are shown on the log-log plot in Figure 15. These plots were generated by measuring the emission intensity of the peak maximum for each spectrum as a function of f. The graph shows slightly curved plots with a linear power dependence of the 1.4-eV emission band at low f followed by a sublinear power dependence at high f. The average slopes at low f and high f for each plot are: 1.1 and 0.52 for the Mn-doped sample, and 1.04 and 0.5 for the undoped sample. According to Taguchi et al. (4) and Feng et al. (5), a slope of value 1 is characteristic of DAP and FB transitions which is inconsistent with the slope values just presented. It seems however, that these authors only took into account the straight line portion of their log-log plots and may have ignored a possible overall curved behavior.

Other experimental data showed a more pronounced curvature with a linear and sublinear power dependence of the 1.4-eV emission band at lower f and higher f, respectively. That is, the slopes at low f and high f were slightly larger than 1 and 0.5, respectively. It will be shown in the Further Discussion section that the slope values calculated above are consistent with the theoretical formulation of the two-hole

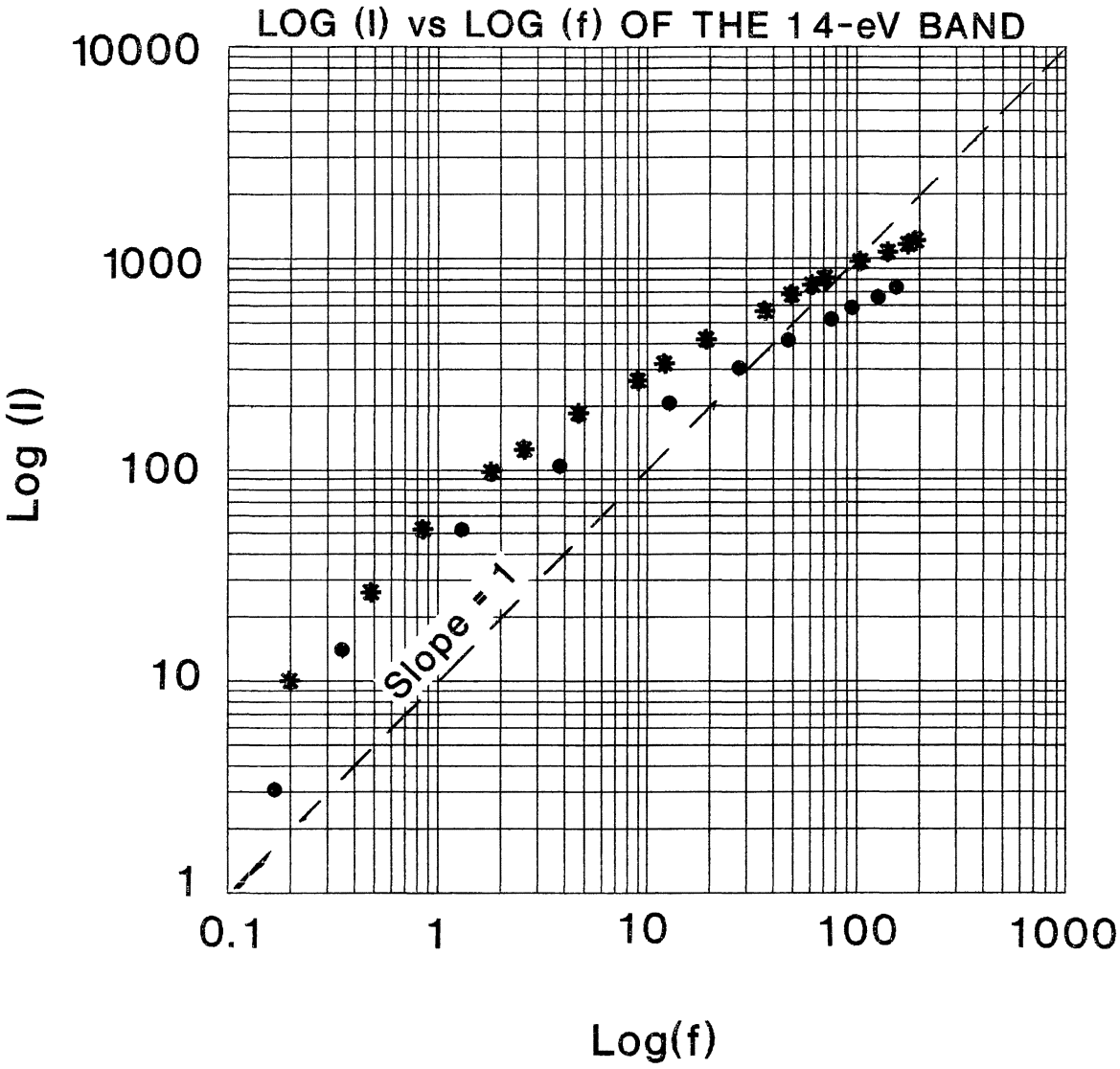

Figure 15. Dependence of the Emission Intensity on the Excitation Intensity Data from the Sample in Fig. 14 (•) and an Undoped Sample (*)

state system which describes FB transitions.

From the time-resolved spectroscopy measurements, a shift in energy is also observed with time after the end of the excitation pulse at 77 K, as shown in Figure 16. In this situation, an apparent shift in energy occurs from higher energies to lower energies with decay time. The shift takes place from 1.47 eV (844 nm) at 0 μs to 1.44 eV (860 nm) at 15 μs. From these spectra, the two overlapping emission components are difficult to discern since the limunescence signal dramatically decreased in intensity as a result of the impedance matching mentioned in Chapter II. Figure 17 illustrates time-resolved spectra that were obtained at 14 K with the same decay times as those shown from the spectra taken at 77 K. Here it is clearly seen how each emission component from each spectrum behaves as a function of decay time. In particular, it is seen that the intensities of the 1.47- and 1.49-eV emission bands dominate the overall emission band at shorter decay times but become less dominating at longer decay times. From these measurements, time constants of about 4 and 3.5 μs were estimated for the intensity decay of each overlapping emission component (i.e., the 1.47 and 1.49 eV peaks). These values were estimated by multiplying the maximum luminescence intensity of each component by e^{-1} in Figure 17. The multiplication factor e^{-1} used in this simple calculation is due to the signal transients of the luminescence which showed a fair exponential decay. Taguchi _et al_. (4), measured a time constant of 4.5 μs for the overall peak

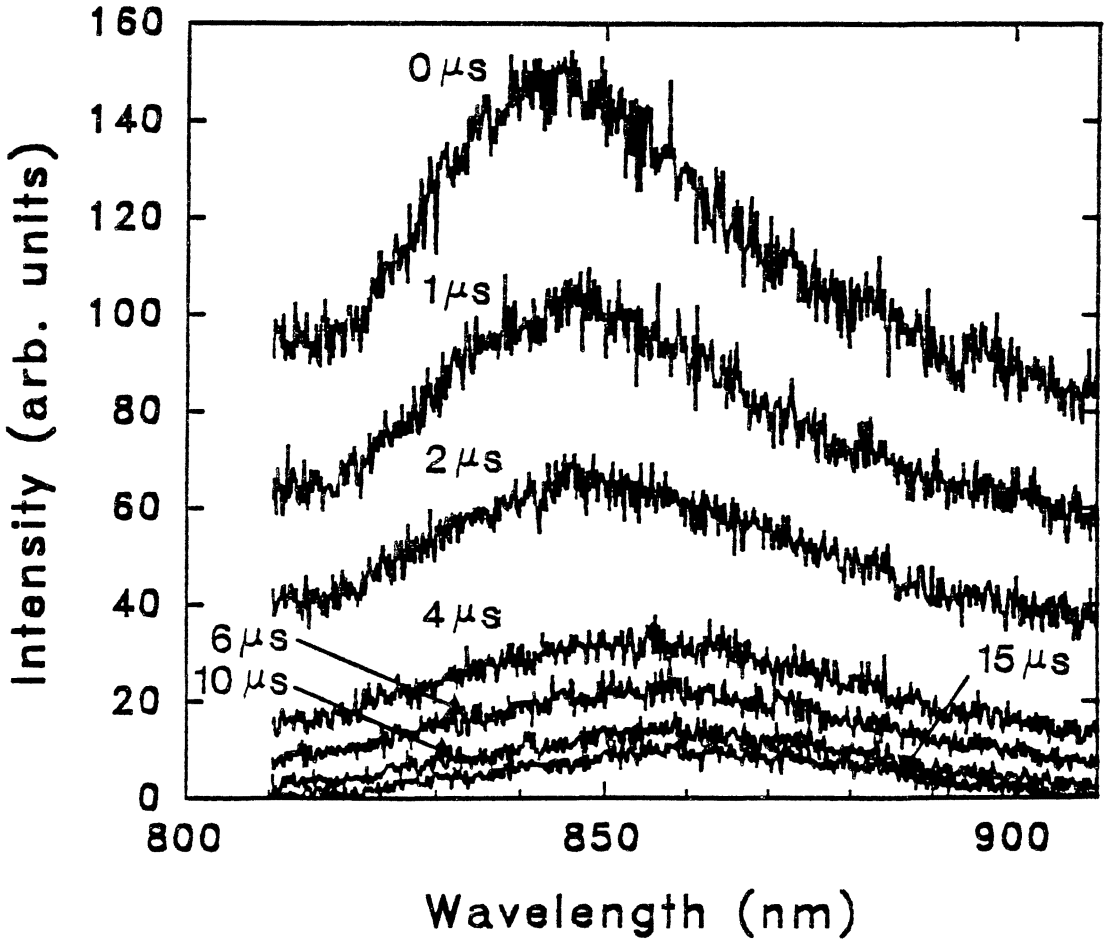

Figure 16. Time-Resolved Spectra at 77 K of the 1.4-eV Emission from an Undoped CdTe Sample

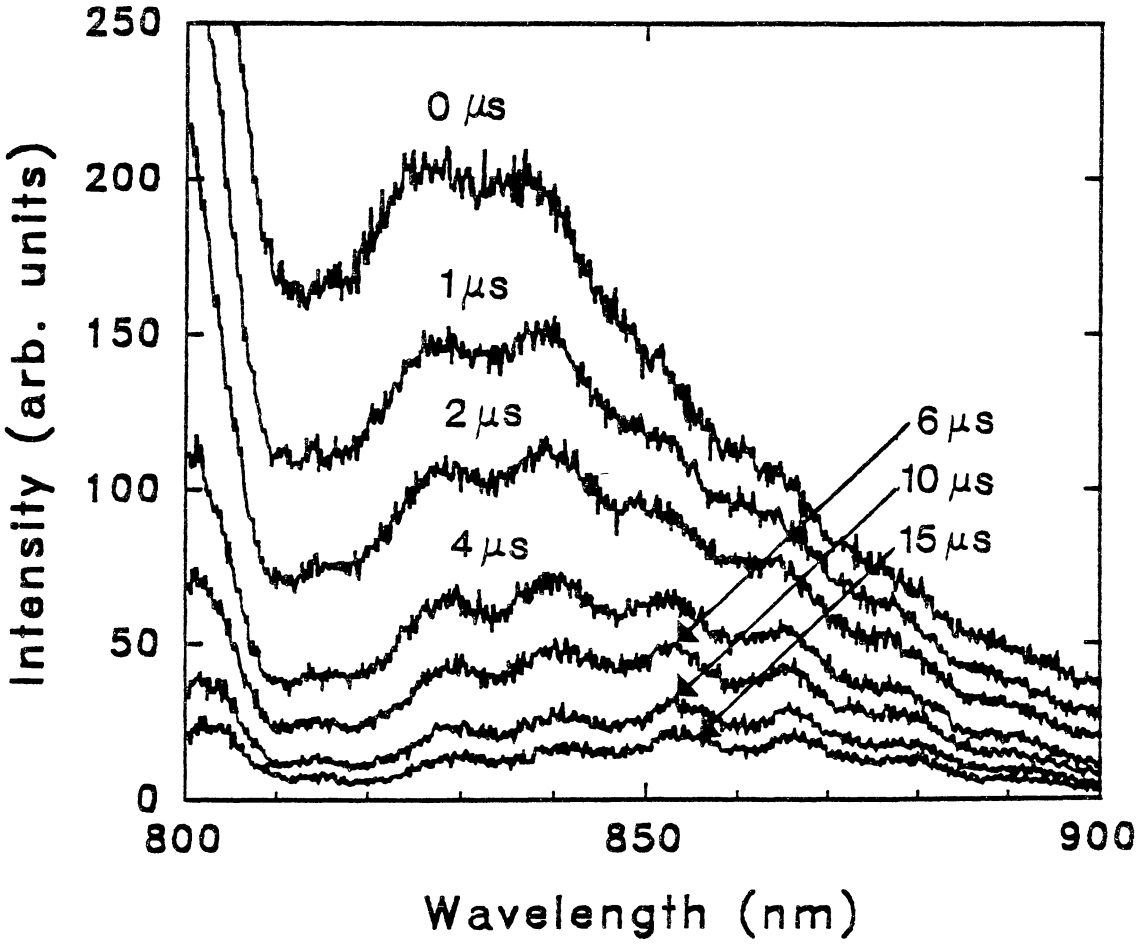

Figure 17. Time-Resolved Spectra at 14 K from the Same Sample in Fig. 16

maximum of the 1.4-eV luminescence band from an undoped, p-type sample. This value of the time constant is close to the values just estimated in the present study. Lifetimes of the order of microseconds are present in the broad-emission band due to the repeated trapping of free electrons and holes by the localized states from the delocalized bands. As a result, the time constant becomes long as the free carrier lifetime increases.

The shifts in energy just noted above were also present in the doped samples. However, since there were weakly overlapping emission peaks, the shifts in energy were not as apparent as that seen in the undoped material. The vapor phase material on the other hand, which also showed little phonon structure, did not show an apparent shift. The reason for this may be due to the lack of overlapping peaks.

It should be mentioned that the energy shifts seen from the time-resolved measurements obtained in this study are in support with the frequency-resolved cathodoluminescence measurements made by Norris and Barnes, (12), and with the time-resolved experiments made by Taguchi et al. (4). However, it should be pointed out that the interpretation of the mechanism responsible for luminescence by the latter authors differs from that of the present study.

Further Discussion

In order to predict the observations from excitation intensity and time-resolved measurements, a set of coupled,

first-order, differential equations will be used to describe the traffic of charge between the energy levels shown in the model of the previous chapter. These equations are:

$$\frac{dn_c}{dt} = f - n_c(N - n)A - n_c n_{h_1} A_{r_1} - n_c n_{h_2} A_{r_2}, \tag{4.1}$$

$$\frac{dn_v}{dt} = f - n_v(N_{h_1} - n_{h_1})A_{h_1} - n_v(N_{h_2} - n_{h_2})A_{h_2}, \tag{4.2}$$

$$\frac{dn}{dt} = n_c(N - n)A, \tag{4.3}$$

$$\frac{dn_{h_1}}{dt} = n_v(N_{h_1} - n_{h_1})A_{h_1} - n_c n_{h_1} A_{r_1}, \tag{4.4}$$

$$\frac{dn_{h_2}}{dt} = n_v(N_{h_2} - n_{h_2})A_{h_2} - n_c n_{h_2} A_{r_2}. \tag{4.5}$$

Here n_c and n_v are the free electron and hole concentrations (cm^{-3}); n is the trapped electron concentration (cm^{-3}); n_{h1} and n_{h2} are the trapped hole concentrations at the two hole levels (cm^{-3}); A, A_{h1} and A_{h2} are the trapping transition probabilities ($cm^{-3}\ s^{-1}$); A_{r1} and A_{r2} are the electron-hole recombination transition probabilities ($cm^{-3}\ s^{-1}$); N, N_{h1} and N_{h2} are the concentrations (cm^{-3}) of available electron and hole traps; and f is the generation rate ($cm^{-3}\ s^{-1}$) of free electrons and holes due to the intensity of the excitation source.

Two emission components denoted as I_1 and I_2 will be used throughout this analysis although more emission peaks could exist in reality. Since the luminescence intensities of these two peaks are directly proportional to the recombina-

tion rate, then

$$I_1 = n_c n_{h_1} A_{r_1} \tag{4.6}$$

and

$$I_2 = n_c n_{h_2} A_{r_2}, \tag{4.7}$$

where for the present study, I_1 is denoted as the intensity of the lower-energy emission component and I_2 as the higher-energy component.

In order to simulate the time-resolved measurements with the above equations, it was assumed, for simplicity, that the illumination occured at low enough temperatures so that the thermal release of trapped carriers could be ignored. This corresponded to neglecting transitions 5-7 and 9 from the proposed model in Figure 13.

The simulation was done in such a way that free electrons and holes were generated by the excitation source according to Eqs. (4.1)-(4.5), with initial concentrations equal to zero. These equations were solved numerically by using a Runge-Kutta, fourth-order, predictor-corrector method where the luminescence intensities I_1 and I_2 were allowed to build up until a steady-state process was reached. At this point, f was set equal to zero and the luminescence decay of I_1 and I_2 were monitored as functions of time.

The excitation intensity measurements were simulated by using the same set of equations employed in the above calculations. However, in these measurements, the steady-state

values of I_1 and I_2 were monitored for several different values of f.

Figure 18 shows some typical results for the following set of parameters: $A = A_{h1} = A_{h2} = 1X10^{-10}$ cm^3 s^{-1}; $A_{r1} = 1X10^{-11}$ cm^3 s^{-1}; $A_{r2} = 2.3X10^{-12}$ cm^3 s^{-1}; $N = N_{h2} = 1X10^{15}$ cm^3; $N_{h1} = 3X10^{14}$ cm^3. In part (a) of the figure, $f = 1X10^{18}$ cm^{-3} s^{-1} and in part (b), f = 0. In part (a) is shown the buildup of I_1 and I_2 versus time after the end of the pulsed excitation source whereas in part (b) is shown the decay of I_1 and I_2. Due to the differences in intensities, it can be seen that I_2 builds up to a larger intensity than I_1 in part (a) but then decays with a faster lifetime in part (b). If the emission peaks of I_1 and I_2 are strongly overlapping, then, in a real experiment, an apparent shift of the overall emission band would be observed as a function of time and would occur from higher energies to lower energies. Figures 15 and 16 show this to be true and it has also been observed in other experimental studies (4).

It should be pointed out that the results shown in Figure 18 were obtained for the specific set of parameters used above. However, it is not necessary that the intensities of I_1 and I_2 actually cross during the decay in order to produce a shift in energy of the overall emission band. What is important is that I_1 and I_2 must have different lifetimes. It should also be noted that sets of parameters were found which did not show a crossing in I_1 and I_2. However, almost every set of calculations that were performed showed differ-

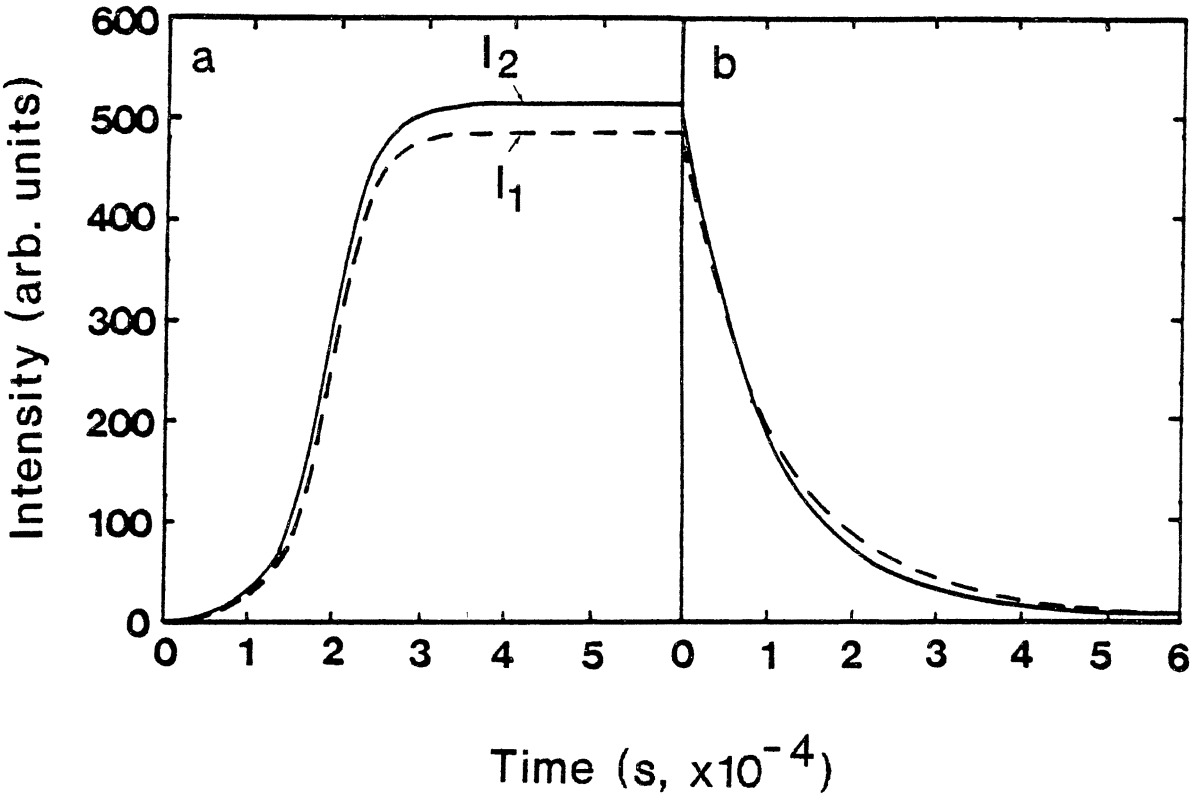

Figure 18. (a) The Buildup of I_1 and I_2 and the (b) Decay of I_1 and I_2 During and After Illumination

ent lifetimes depending upon the relative sizes of N_{h1} and N_{h2}, and the corresponding values of the trapping and recombination probalities.

In Figure 19 is shown the dependence of I_1 and I_2 on excitation intensity, f. Here it is demonstrated that if I_1 and I_2 are at different wavelengths (energies), then an apparent shift in energy of the overall emission band will be observed as one component begins to dominate over the other. This shift will occur from lower energy to higher energy (i.e., I_1 and I_2), as f increases. It is not necessary that the two lines in Figure 19 cross each other in order to predict a shift in energy. What is required is that the two lines must have different slopes. These results were confirmed from Figure 14 and were also observed in other experimental work (12,14). As pointed out above, different behavior can be obtained for a different set of parameters. For instance, the inset to Figure 19 shows that situations in which the ratio of I_1 and I_2 remains constant can be obtained over a range of f. On the other hand, different ranges of f can be obtained in which the ratio of I_1 and I_2 does not remain constant. Thus, these calculations illustrate that the model is capable of producing the experimental behavior seen in practice.

It should be mentioned that the values of the parameters used in the above calculation are believed to be realistic, but are not meant to be indicative of CdTe. By slightly changing the relative concentrations of available states

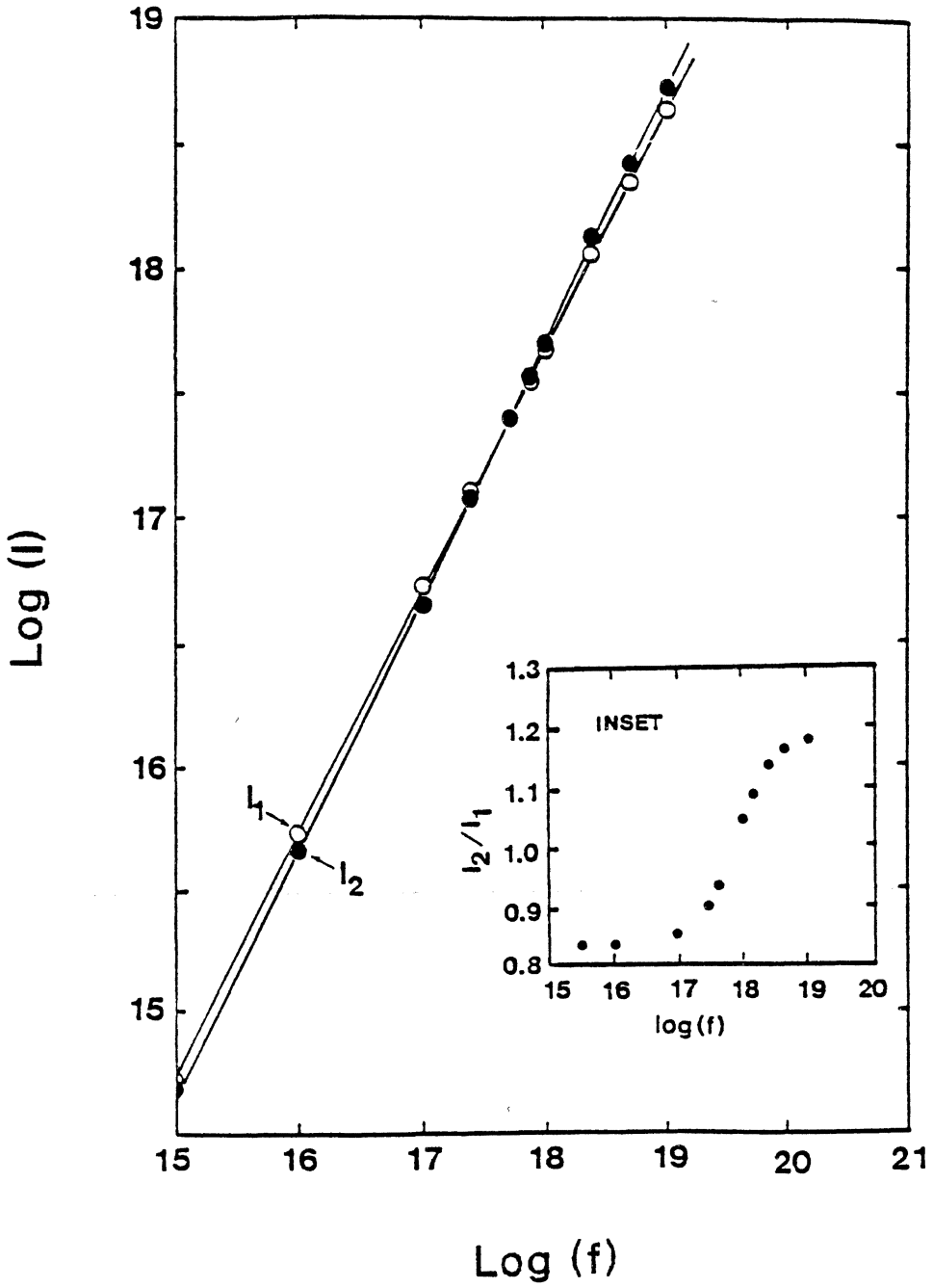

Figure 19. Variation of Steady-State Values of I_1 and I_2 with f

(i.e., by factors of 2 or 3), different behavior from the values of I_1 and I_2 were noted.

The following theoretical formulation will be presented in order to explain the linear to sublinear power dependence of the 1.4-eV luminescence intensity data shown in Figure 15. That is, for FB transitions the slope changes from n = 1 to n < 1 as f increases. First, by assuming only one component, Equations (4.1) to (4.5) become,

$$\frac{dn_c}{dt} = f - n_c(N - n)A - n_c n_h A_r; \tag{4.8}$$

$$\frac{dn}{dt} = n_c(N - n)A; \tag{4.9}$$

$$\frac{dn_v}{dt} = f - n_v(N_h - n_h)A_h; \tag{4.10}$$

$$\frac{dn_h}{dt} = n_v(N_h - n_h)A_h - n_c n_h A_r. \tag{4.11}$$

(Note that these equations ignore exciton formation.) At equilibrium, all the $\frac{d}{dt}$'s = 0, thus

$$n_c(N - n)A = 0 \tag{4.12}$$

and

$$f = n_v(N_h - n_h)A_h = n_c n_v A_r. \tag{4.13}$$

Since $I = n_c n_h A_r$, then I = f and a linear f dependence is obtained.

However, in a real system the exciton formation has to be considered. The equations are modified as

$$\frac{dn_c}{dt} = f - n_c n_v A_e - n_c(N - n)A - n_c n_h A_r \tag{4.14}$$

and

$$\frac{dn_v}{dt} = f - n_c n_v A_e - n_v(N_h - n_h)A_h \qquad (4.15)$$

where A_e is the probability of free exciton formation. (Note that it is likely that $A_e << A_r$.) Charge neutrality for semi-pure materials (this may not be true for highly impure materials since $n + n_c = n_v + n_h$ -- but all of the materials used in this work are semi-insulating) impies that

$$n_c = n_v. \qquad (4.16)$$

At equilibrium

$$\begin{aligned} f &= n_c n_v A_e - n_c n_h A_r \\ &= n_c^2 A_e - n_c n_h A_r. \end{aligned} \qquad (4.17)$$

Recall that

$$n_v(N_h - n_h)A_h = n_c n_h A_r \qquad (4.18)$$

or

$$\frac{n_h}{(N_h - n_h)} = \frac{A_h}{A_r}. \qquad (4.19)$$

Since N_h, A_h and A_r are all constants of the system then n_h is constant, independent of f, at equilibrium.

At low f, we may have $n_c n_h A_r >> n_c^2 A_e$ (recall $A_r >> A_e$) so that $f = n_c n_h A_r$, and consequently, $f \propto n_c$. Thus,

$$I = f \qquad (4.20)$$

as before.

At high f, as n_c increases, it is possible to have $n_c^2 A_e >> n_c n_h A_h$ so

$$f = n_c^2 A_e \propto n^2. \tag{4.21}$$

Thus

$$I = n_c n_h A_h \propto f^{1/2} \tag{4.22}$$

since $n_h A_h$ is a constant (i.e., independent of f). Hence, the above discussion shows that the intensity goes from $I \propto f$ at low f to $I \propto f^{1/2}$ at high f which is in agreement with the experimental results.

The above rate equation formulation was done for only one component. For two components, the analysis would entail using Equations (4.1) to (4.5) but the results would be the same.

CHAPTER V

SUMMARY AND CONCLUSIONS

Photoluminescence thermal quenching, excitation intensity dependence and time-resolved spectroscopy measurements were used in this study to characterize the localized defect states in CdTe. The data obtained from these experimental techniques provided much information on the radiative recombination mechanisms responsible for the 1.4-eV emission. This information suggested the need of a model to explain the experimental evidence obtained in the present work (and by other authors) which included the existence of overlapping emission components in the 1.4-eV emission region.

The two-hole-state model was shown to explain the PL and thermal quenching results. From this model (figure 13), it was postulated that transitons 5 and 7 were due to the thermal release of trapped holes to the valence band with activation energies of 0.13 and 0.11 eV, respectively . The interlevel transition (transition 6) was due to the thermal release of a trapped hole from the deeper hole state to the shallower state with an activation energy of 0.02 eV. As a result of hole trapping (transitions 3 and 5), the 1.47 and 1.49 eV emission components (i.e. transitions 1 and 2) were made possible via electron-hole recombination. It was noted

from reference (19) that TSC was observed during transitions 5 and 7 but no TSC was observed for the interlevel transiton.

From excitation intensity dependence studies, it was observed that a shift in energy of the 1.4-eV emission band occured from lower energies to higher energies as the excitation power increased. It was noted that the model could not account for the shift in energy if only one hole state was present. This was also observed to be the case in cathodoluminescence studies performed by Norris and Barnes (12).

The work of Taguchi et al. seems to be the only experimental time-resolved spectroscopy study on the 1.4-eV defect band reported in the literature. A shift in the position of the band from higher energy to lower energy was seen by these authors as a function of time after the end of the excitation pulse but no correlation with overlapping peaks was made. Based on the model proposed here, it is inferred that more than one emission component was present from the samples used in that study.

By solving a set of coupled, first-order, differential equations describing the flow of charge in the model of Figure 13, shifts in energy of the overall peak maximum were predicted as a function of excitation intensity and time after the cessation of the excitation pulse. These predictions are possible only if overlapping emission components are present in the defect band.

It is important to point out that the two-hole-state model presented in this study should not be strictly consid-

ered as the only model. In real crystals, three or more hole states may be present thus complicating the mechanism of the system. Whatever the case may be, it should be noted that the simple model can be adjusted in a straightforward manner to include more than two hole states.

Finally, it was shown that surface damage introduces defect states which reduce the overall PL emission. This was easily handled in the model by incorporating trapped electron states for which free holes could recombine nonradiatively. From TSC measurements one such electron state was observed with a trap depth of 0.21 eV below the conduction band (19). These nonradiative pathways are believed to present alternative recombination possibilities for the holes. In the presence of such centers a weaker luminescence signal would occur. This is suspected to be the cause of the variability in the emission as a result of surface treatments, as noted in this study and as observed by Myers et al. (13).

A major thrust has been directed in determining the defect nature of the 1.4-eV luminescence band in the past few years. However, to this date, no definite agreement has been reached as to the defect origin of this band. Perhaps by using the ideas from the model presented in this work, it may help provide further insight as to the defect responsible for the 1.4-eV emission in future work. Nevertheless, the model is capable of explaining most of the results reported for this emission in CdTe when free-electron to trapped-hole

recombination transitions are taken into account with hole states a few hundreths of an electron volt above the valence band. It is stressed that the existence of overlapping emission peaks is a crucial factor in this description and that the presence of competing, nonradiative pathways (due to surface damage) can result in dramatic changes in the 1.4-eV luminescence from sample to sample, and as a function of surface treatment.

LITERATURE CITED

1. Frerichs, R., Phys. Rev. 72, 594 (1947).

2. De Nobel, D., Philips Res. Rep. 14, 361 (1959).

3. Thomas, D. G., J. Appl. Phys. Suppl. 32, 2298 (1961).

4. Taguchi, T., J. Shirafuji, and Y. Inuishi, Jap. J. Appl.Phys. 12, 1558 (1973).

5. Feng, Z. C., A. Mascarenhas, and W. J. Choyke, J. Lumin. 35, 329 (1986).

6. Ohba, K., T. Taguchi, C. Onodera, Y. Hiratate, and A. Hiraki, J. Appl. Phys. 28, 1246 (1989).

7. Panosyan, Zh. R., "Radiative Recombination in Semiconducting Crystals," in Proceedings (Trudy) of the P. N. Lebedev Physics Institute, Moscow, 1975, ed. by A. D. V. Skobel'tsyn (Director, P. N. Lebedev Physics Institute Academy of Sciences of the USSR, Moscow), 145.

8. Furgolle, B., M. Hoclet, M. Vadevyver, Y. Marfaing, and R. Triboulet, Solid State Commun. 14, 1237 (1974).

9. Zanio, K. R., "Semiconductors and Semimetals," ed. by R. K. Willardson and B. C. Beer (Academic Press, New York, 1978), vol. 13.

10. Chamonal, J. P., E. Molva, and J. L. Pautrat, Solid State Commun. 43, 801 (1982).

11. Agrinskaya, N. V., E. N. Arkad'eva, and O. A. Matveev, Sov. Phys. Semicond. 5, 767 (1971).

12. Norris, C. B., and C. E. Barnes, Rev. Phys. Appl. 12, 219 (1977).

13. Myers, T. H., J. F. Schetzina, S. T. Edwards, and A. F. Schreiner, J. Appl. Phys.54, 4232 (1983).

14. Espinosa, J. E., J. M. Garcia, H. Navaro, and A. Zehe, J. Lumin. 28, 163 (1983).

15. Barnes, C. E., and K. R. Zanio, J. Appl. Phys. 46, 3959 (1975).

16. Norris, C. B., and K. R. Zanio, J. Appl. Phys. 53, 6343 (1982).

17. Norris, C. B., J. Appl. Phys. 51, 6342 (1980).

18. Morrison, R., "Grounding and Shielding Techniques in Instrumentation," (Wiley, New York, 1986).

19. Cotal, H. L., A. C. Lewandowski, B. G. Markey, S. W. S. McKeever, E. Cantwell, and J. Aldridge, J. Appl. Phys. 67(2), 975 (1989).

20. Kittel, C., "Introduction to solid State Physics," (Wiley, New York, 1986).

21. McKeever, S. W. S., "Thermoluminescence of Solids," (Cambridge University Press, Cambridge, 1985).

22. Hopfield, J. J., J. Phys. Chem. Solids 10, 110 (1959).

VITA

Hector Luis Cotal

Candidate for the Degree of

Master of Science

Thesis: 1.4-EV LUMINESCENCE IN P-TYPE CADMIUM TELLURIDE SINGLE CRYSTALS

Major Field: Physics

Biographical:

Personal Data: Born in Aguadilla, Puerto Rico, February 12, 1959, the son of Pete Cotal and Elba Zapata. Married to Sharon Ann Isbell on June 21, 1986.

Education: Graduated from Dr. Pila High School, Ponce, Puerto Rico, in May 1979; received the Bachelor of Science degree in Physics from Oklahoma State University in July, 1986; completed the requirements for the Master of Science degree at Oklahoma State University in July, 1990.

Professional Experience: Graduate Teaching Assistant, Oklahoma State University, August, 1987 to May, 1988; Graduate Research Assistant, Oklahoma State University, June, 1988 to present; Member of the American Physical Society and the Optical Society of America.